Ore Geology Reviews 78 (2016) 41–57

Contents lists available at ScienceDirect

Ore Geology Reviews

journal homepage: www.elsevier.com/locate/oregeorev

Mineral assemblages, fluid evolution, and genesis of polymetallic epithermal veins, Glojeh district, NW Iran

Behzad Mehrabi [a,*], Majid Ghasemi Siani [a], Richard Goldfarb [b], Hossein Azizi [c], Morgan Ganerod [d], Erin Elizabeth Marsh [b]

[a] Department of Geochemistry, Faculty of Earth Sciences, Kharazmi University, Tehran, Iran
[b] United States Geological Survey, Box 25046, MS 973, Denver Federal Center, Denver, CO 80225, USA
[c] Mining Department, Faculty of Engineering, University of Kurdistan, Sanandaj, Iran
[d] Geological Survey of Norway (NGU), Leiv Eirikssons vei 39, 7491 Trondheim, Norway

ARTICLE INFO

Article history:
Received 28 May 2015
Received in revised form 18 March 2016
Accepted 19 March 2016
Available online 30 March 2016

Keywords:
Glojeh epithermal veins
Fluid inclusion
Stable isotope
Geochronology
Mineralization
Fluid evolution
Genesis

ABSTRACT

The Glojeh district contains silver- and base metal-rich epithermal veins and is one of the most highly mineralized locations in the Tarom-Hashtjin metallogenic province, northwestern Iran. It consists of four major epithermal veins, which are located in the South Glojeh and North Glojeh areas. Alteration in the Glojeh district consists of propylitic, sericitic, and argillic assemblages, as well as extensive silicification. The ore-bearing veins comprise three paragenetic stages: (1) early Cu-Au-As-Sb-Fe-bearing minerals, (2) middle stage Pb-Zn-Cu-Cd-Ag-bearing minerals, and (3) late hematite-Ag-Bi-Au-Pb mineralogy. The veins are best classified as the product of an early high-sulfidation hydrothermal system, which was overprinted by an intermediate sulfidation system that was rich in Ag and base metals. Hematite is locally altered to goethite in zones of as much as 40 m in width during supergene alteration and the goethite is an important exploration tool. Fluid inclusions from the early, middle, and late stages, respectively, have salinities and homogenizations temperatures ranging from 5 to 11 wt.% NaCl eq. and 220 °C to 340 °C, to 1 to 8 wt.% NaCl eq. and 200 °C to 290 °C and finally to. 0.1 to 2 wt.% NaCl eq. and 150 °C to 200 °C. The oxygen isotope values in quartz range from 8.8 to 13.3‰ and most calculated fluid $\delta^{18}O$ values are between 4 and 8‰, suggesting a magmatic fluid with some meteoric water contamination. Sulfur isotope values for chalcopyrite, pyrite, sphalerite, and galena are mainly −7.3 to +1.3‰ and −0.3 to +8.4‰ for North Glojeh and South Glojeh, respectively. Sulfur isotope data suggest a magmatic origin. Boiling, isothermal mixing, and dilution are the main mechanisms for ore deposition in the Glojeh veins. Recent $^{40}Ar/^{39}Ar$ age measurements of 42.20 ± 0.34 Ma and 42.56 ± 1.47 Ma for the North Glojeh and South Glojeh veins, respectively, overlap with the 41.87 ± 1.58 Ma age of the Goljin intrusion in the northern part of the district, which we interpret as the main heat source controlling the hydrothermal systems.

1. Introduction

The east-west trending Alborz Magmatic Belt in northern Iran (Azizi and Moinevaziri, 2009; Azizi and Jahangiri, 2008) is divided into western and eastern parts by the north-south striking Rasht-Takestan Fault (Fig. 1). The eastern part consists of mafic and felsic tuff and lava with an alkaline to shoshonitic affinity (Nabatian and Ghaderi, 2013; Nabatian et al., 2014; Moayyed, 2001; Blourian, 1994), whereas the western part consists of andesitic to dacitic lava and many calc-alkaline to shoshonitic granitoid bodies. The western part, referred to here as the Alborz-Azarbayejan Magmatic Belt, is subdivided into two mineralized provinces, the Ahar-Arasbaran Belt in the north and the Tarom-Hashtjin metallogenic province in the south (Fig. 1).

The Glojeh district is situated approximately 30 km north of the town of Zanjan, within the Tarom-Hashtjin metallogenic province (Fig. 2). The district consists of a set of polymetallic (Pb-Zn-Cu-Ag-Au) sulfide-bearing veins, with also recoverable amounts of Cd and Bi. It can be subdivided into a northern area of silver and base metal-rich veins that trend east-west, and a southern area of gold-rich veins that are NW-and N-S-trending (Fig. 3). No modern-day mining has occurred in the Glojeh district, except for the Cu-Au Rasht Abad deposits that are located in 250 m east of the North Glojeh veins. However, historic mine workings can be seen as tunnels and wells in the North Glojeh area. Modern exploration in the Glojeh district has been conducted by the Iranian Mineral Research and Application Co. (IMRA) since 2003. In 2003, exploration drilling led to the discovery of the northern group of veins, which motivated an extensive exploration program in the area that resulted in the discovery of southern veins in 2005. In 2006, the IMRA estimated a combined reserve for the district of

* Corresponding author.
E-mail address: mehrabi@khu.ac.ir (B. Mehrabi).

http://dx.doi.org/10.1016/j.oregeorev.2016.03.016
0169-1368/

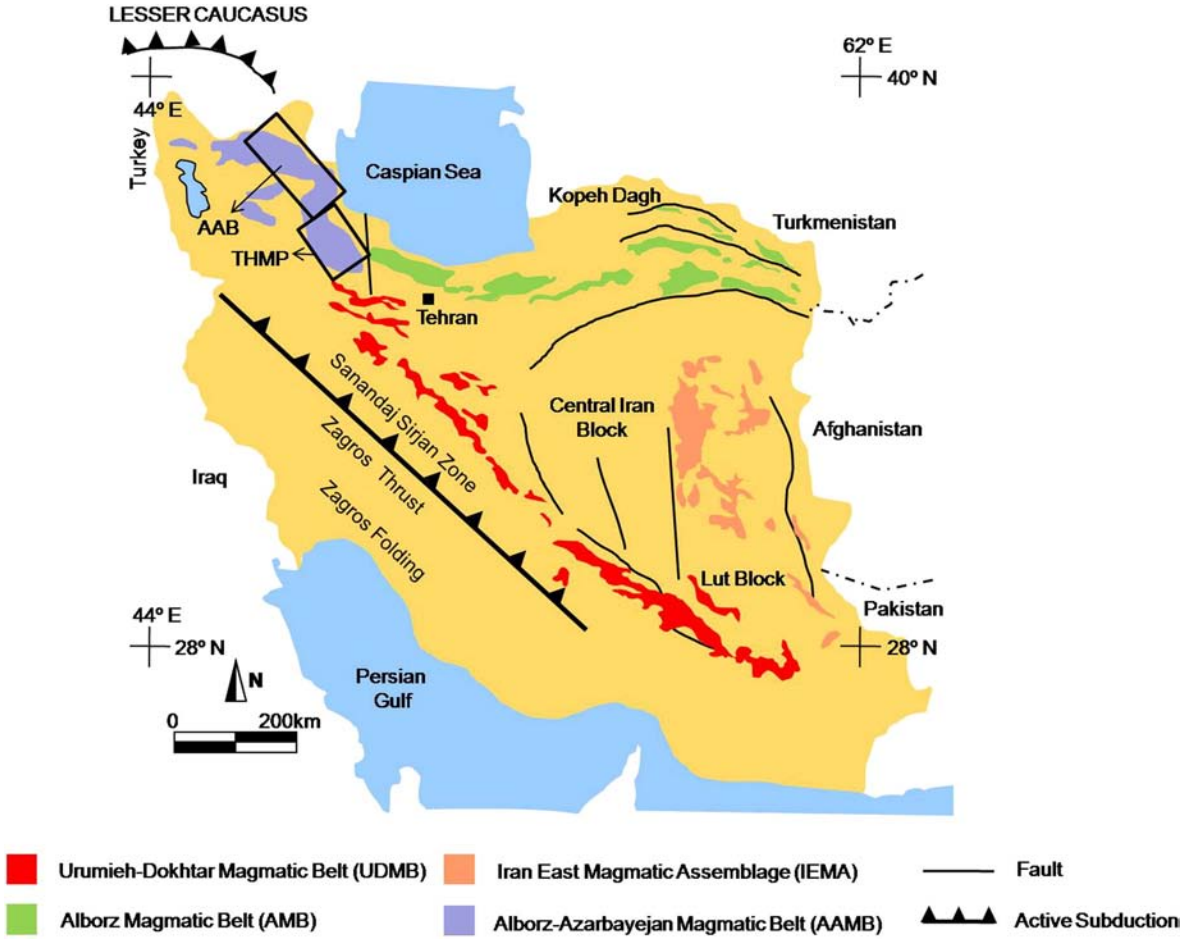

Fig. 1. Location of the Tarom-Hashtjin metallogenic province in the Alborz-Azarbayejan Magmatic Belt (NW Iran). The Alborz-Azarbayejan Magmatic Belt is subdivided into the Ahar-Arasbaran Belt in the north and Tarom-Hashtjin metallogenic province in the south.

2.27 million tonnes of ore containing an average grade of 3.0% Pb, 2.2% Zn, 1.5% Cu, 2.88 g/t Au, and 350 g/t Ag.

In this paper, we present a detailed study on the geology, paragenesis, hydrothermal alteration, fluid inclusion characteristics, and stable isotope geochemistry of the ore veins. The characteristics of the mineralized veins in both the northern and southern Glojeh areas are used to suggest an ore genesis model. This paper builds upon what was first published by Mehrabi et al. (2014), which introduced the North Glojeh veins as epithermal mineralization. In this paper, we have added new data on the hydrothermal alteration, fluid inclusion characteristics, geochronology, and stable isotope geochemistry of both the North Glojeh and South Glojeh veins for comparative purposes, and for development of a comprehensive regional ore formation model.

2. Regional geology

The Alborz magmatic belt is situated in northern Iran and has an E-W orientation, and is 600 km in length and 100-km-wide. The Alborz magmatic belt occurs in the hinterland of the Arabian-Eurasia collision zone in the broad Alpine-Himalayan orogenic belt. The Sanandaj-Sirjan zone formed as a result of the subduction of Neotethys ocean crust during the Mesozoic. Subsequently a back-arc basin developed behind the Sanandaj-Sirjan zone. This back-arc basin was subducted beneath the Central Iran block, and the Urmieh-Dokhtar magmatic belt formed along the continental margin of central Iran. High-angle subduction in the northwestern part of Iran (Azizi and Jahangiri, 2008) caused the development of an extensional tectonic regime in the Alborz-Azarbayejan micro-continent. Subduction of Neotethys beneath central Iran ended in the Late Cretaceous-early Paleocene with collision of the Sanandaj-Sirjan zone with the Central Iran block. During this period, the Khoy back-arc basin began subduction to the northeast beneath the Alborz-Azarbayejan micro-continent (Azizi and Jahangiri, 2008; Juteau, 2003; Ghazi et al., 2003; Khalatbari-Jafari et al., 2003). The result of this subduction was the formation of the Alborz-Azarbayejan magmatic belt. This subduction occurred during the early Eocene and, due to emplacement of several intrusive bodies near the end of subduction, resulted in widespread mineralization in the Alborz-Azarbayejan Magmatic Belt. In the Alborz magmatic belt, the bedrock consists of a Paleozoic-Mesozoic passive-margin sedimentary sequence with few volcanic rocks, overlain, in the south, by Cenozoic volcanic and sedimentary rocks (Mirnejad et al., 2010). Cenozoic successions in the Alborz magmatic belt are represented mainly by marine and subaerial, porphyritic and non-porphyritic, massive lava flows of andesite, basaltic andesite, and basalt (Aghazadeh et al., 2010, 2011). In addition, the Alborz-Azarbayejan magmatic belt can be subdivided into two metallogenic regions, termed the Ahar-Arasbaran metallogenic belt (AAB) in the north and the Tarom-Hashtjin metallogenic province (THMP) in the south (Fig. 1).

The Glojeh district is located approximately in the middle of the Tarom-Hashtjin metallogenic province (Fig. 2), where it abuts the NW-trending Urmieh-Dokhtar volcano-plutonic zone that parallels the Zagros thrust-fault system (Fig. 1). The NW-striking metallogenic province, 70- to 150-km-wide and 300-km-long, hosts numerous Ag-Au and polymetallic epithermal deposits associated with Eocene to Oligocene volcanic and plutonic events (Fig. 2). Regionally, the Tarom-Hashtjin metallogenic province is underlain by Precambrian metamorphic basement, Cambrian and Permian metamorphic rocks, Jurassic to

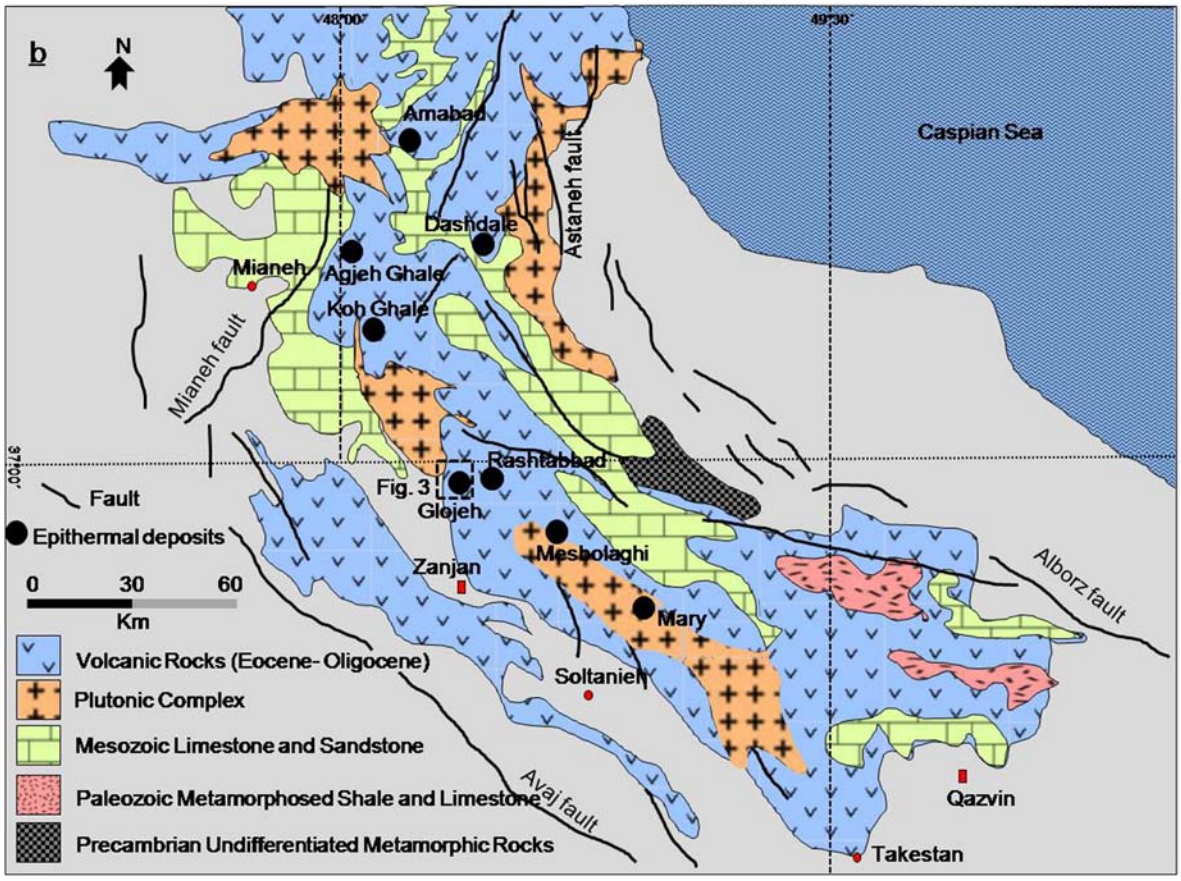

Fig. 2. Regional geology of the Tarom-Hashtjin metallogenic province showing major stratigraphic units, and location of the Glojeh polymetallic district and other epithermal deposits.

Cretaceous limestone and sandstone, and the Eocene to Oligocene volcano-plutonic rocks (Fig. 2).

3. District geology

Three major Cenozoic igneous units form the country rocks to the mineralization in the Glojeh district (Fig. 3; Geological Survey of Iran, 2005). A pervasively well-layered lithic tuff unit is composed of mostly quartz phenocrysts, plagioclase, and ubiquitous flattened fragments. A second unit is marked by andesitic basalt with interlayered basic tuff. Andesitic basalt is exposed predominately in the southern part of the district, whereas lithic tuffs are more abundant in northern part of the district. Dark and light brown porphyritic andesitic basalts are composed mostly of andesine, hornblende, clinopyroxene, and minor olivine, with accessory magnetite. Phenocrysts are mainly plagioclase and clinopyroxene. The third unit is rhyodacite, which only occurs in the central and western parts of the Glojeh district (Fig. 3). Rhyodacites are characterized by phenocrysts of mainly clay-altered plagioclase (andesine and oligoclase in composition), and smaller phenocrysts of variably altered alkali feldspar, quartz, and biotite in a matrix rich in alkali feldspar. Several subvolcanic dikes, characterized by quartz, biotite, and plagioclase phenocrysts, intrude the lithic tuff unit. Two granite, granodiorite, and quartz monzonite composite stocks are present at Goljin and Varmarziar (Fig. 3). A younger rhyolite dome intrudes the rhyodacites in the western part of the district.

The geochemistry and geochronology of igneous rocks in Glojeh district are discussed in detail by Ghasemi Siani et al. (2015), so here we just give a brief summary. Igneous rocks in Glojeh district are classified as high-K calc-alkaline to shoshonitic series. Mineralization in the Glojeh district is associated with these high-K calc-alkaline to shoshonitic volcano-plutonic rocks, which are highly alkaline (as much as 8.92 wt.% $K_2O + Na_2O$), have high K_2O/Na_2O (0.9 to 1.8 wt.%), low TiO_2 (~1.02 wt.%), and high to variable Al_2O_3 contents (14 to 18 wt.%). The $^{40}Ar/^{39}Ar$ ages of North Glojeh and South Glojeh veins are 42.20 ± 0.34 Ma and 42.56 ± 1.47 Ma, respectively (Ghasemi Siani et al., 2015). A $^{40}Ar/^{39}Ar$ date on biotite of 41.87 ± 1.58 Ma, from the Goljin intrusion, indicates that the emplacement age for the intrusion is contemporaneous with formation of the North Glojeh and South Glojeh mineralized veins (Table 1). Feldspar and biotite from the Varmarziar granodiorite are defined by partially flat Ar release patterns, with mean plateau ages of 39.08 ± 0.37 Ma and 39.07 ± 0.16 Ma, respectively (Table 1).

4. Mineralization

4.1. Mineralization style

The Glojeh district consists of four main polymetallic veins, termed No. 1 and No. 2 in the North Glojeh and A and B in the South Glojeh areas. The veins and several veinlets occupy E-W trending faults and generally dip steeply to the south in the North Glojeh area (Fig. 3). The No. 1 vein is >750 m in length and locally is >4 m in width, although typically averaging a couple of meters. The No. 2 vein is 450 m in length, averages 2 m in width, and is located about 7 m south of the No.1 vein. The two polymetallic veins strike E-W, dip 75–80° to the south, and continue down-dip to depths of 300 m. Furthermore, several veinlets are located between the two main veins in North Glojeh. The two main veins in South Glojeh have different orientations. The A vein occurs over a strike length of 700 m, has an average thickness of 3 m, is nearly N-S-trending, and dips 60–65° to the west. In contrast, the B vein can be followed for about 850 m along a N40°W strike and it dips 65–70° to the southwest. Also in the South Glojeh area, there are two mineralized N-S-striking smaller veins with lengths of 30–40 m and mean widths of 1 m. The silver- and base metal-rich veins in the northern part of the

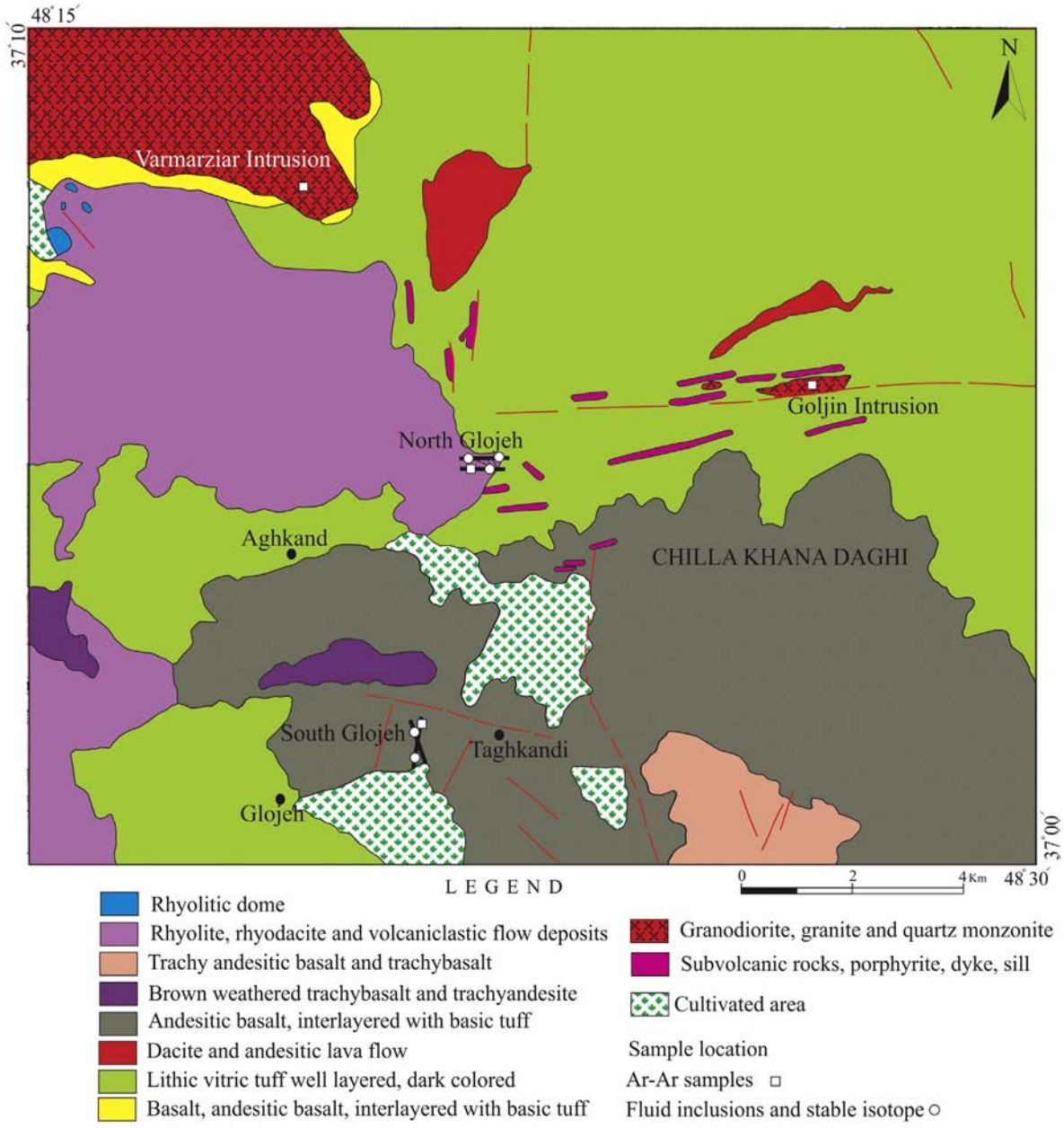

Fig. 3. Simplified geology of the Glojeh district, showing the North Glojeh and the South Glojeh veins and sample locations (modified after Hashtjin quadrangle map provided by Geological Survey of Iran, 2005).

Glojeh district are hosted mainly by the rhyodacite unit, except in the far east where they are contained in the lithic tuff unit. The gold- and base metal-rich veins in the southern part of the district are mostly hosted by the andesitic basalts.

The veins in the Glojeh district comprise fine- to medium-grain quartz that is massive or infills vugs. Crustiform banded (open-space filling) textures are particularly noticeable in the North Glojeh veins associated with the base metal mineralization stage, whereas quartz (up

Table 1
$^{40}Ar/^{39}Ar$ results for CO_2 laser step heating experiments. Ages are in Ma. Uncertainties are reported as analytical errors at 1.96σ level. MSWD (P) denotes mean squared weighted deviance, and P is the probability of fit. TGA denotes Total Gas Age. G1 (South Glojeh), G2 (North Glojeh), F392-3 (Goljin intrusion), F392-5 (Varmarziar intrusion).

Sample	Spectrum analysis						Inverse isochron analysis			
	Steps (n)	%39Ar	Age ± 1.96 σ	MSWD (P)	TGA ± 1.96 σ	K/Ca ± 1.96 σ	Age ± 1.96 σ	MSWD (P)	Intercept ± 1.96 σ	Spread %
F392–5 (Biotite)	2–6 (5)	80.9	39.07 ± 0.16	0.993 (0.41)	39.68 ± 0.15	12.42 ± 0.52	39.09 ± 0.32	1.32 (0.266)	297.0 ± 27.14	16.8
F392–5 (Feldspar)	2–6 (5)	92.63	39.08 ± 0.37	0.375 (0.826)	38.64 ± 0.95	1.2 ± 0.024	38.34 ± 2.51	0.38 (0.767)	314.8 ± 55.85	23.3
F392–3 (Biotite)	4–7 (4)	49.82	41.87 ± 1.58	1.563 (0.196)	39.91 ± 0.83	42.3 ± 26.0	38.47 ± 5.65	0.997 (0.0)	524.05 ± 445.1	13.8
G1 (Feldspar ± sericite)	4–5 (2)	52.18	42.56 ± 1.47	5.295 (0.0)	39.79 ± 1.18	0.3396 ± 0.005	–	–	–	–
G2 (Feldspar ± sericite)	1–4 (3)	82.27	42.20 ± 0.34	2.114 (0.121)	42.51 ± 0.80	100.1 ± 92.7	40.94 ± 1.36	0.193 (0.0)	335.01 ± 39.37	33.8

to 30 vol.%) is predominant in the South Glojeh veins. Replacement and breccias textures, which are most widespread in the North Glojeh veins, are associated with Cu sulfide-rich mineralization. Silicified host rocks and sulfide-bearing quartz stockworks are also more common in the North Glojeh area. Colloform vein texture is associated with precious metals most commonly in the South Glojeh area, and these veins locally exhibit comb texture and may be associated with disseminated ores.

The North Glojeh polymetallic veins are rich in silver, whereas the South Glojeh polymetallic veins are richer in gold. The average Au and Ag concentrations in the North and the South Glojeh veins are 2.1 ppm and 430 ppm, and 2.9 ppm and 73 ppm, respectively, with the highest gold grades mainly associated with the late stage (see below).

4.2. Paragenetic succession

Most of the mineral assemblages in the veins of the North Glojeh and the South Glojeh areas are similar, but there are a few important mineralogical differences between the veins in the two areas. Enargite, native silver, and tetrahedrite are common in North Glojeh, but they are minor or even absent in the South Glojeh veins. The South Glojeh veins, with notably less silver and Cu-bearing sulfide minerals, have a greater gold content and thus higher Au/Ag ratios. As noted above, veins in North Glojeh are characteristically more crustiform banded and also have replacement and breccias textures, whereas massive and colloform textures are more common in the South Glojeh veins. Despite these differences, an overall paragenesis for the veins in the district can be established as: (1) early Cu-Au-As-Sb-Fe-rich minerals, (2) middle Pb-Zn-Cu-Cd-Ag-rich minerals, and (3) late hematite with inclusions of Ag-Bi-Au-Pb-S-rich minerals (Fig. 4).

Stage 1 is subdivided into two sub-stages. Sub-stage 1A is characterized by the deposition of vuggy and massive quartz containing massive to disseminated pyrite and magnetite (Figs. 5c, 6a). Pyrite occurs as euhedral grains, locally corroded, and may be replaced by fine-grained chalcopyrite, sphalerite, and galena during the later sub-stage 1B and stage 2 events. Magnetite is euhedral to anhedral and shows intergrowth with pyrite, and its composition is homogeneous. Sub-stage 1B is characterized by the deposition of a Cu-Au-As-Sb-Fe-bearing mineral

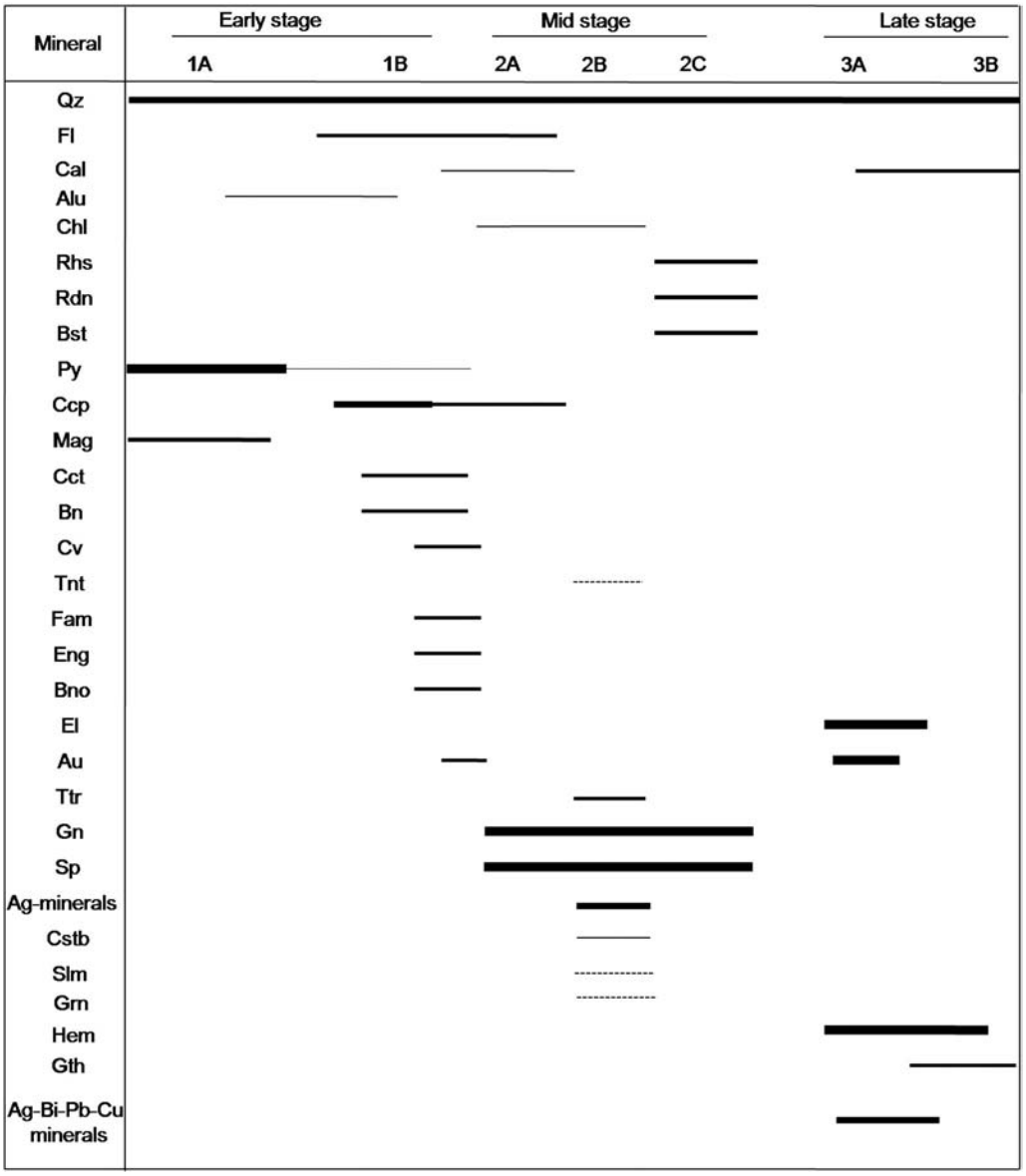

Fig. 4. Paragenetic sequence of ore and gangue minerals in the Glojeh veins. Mineral abbreviations; (Qz) quartz, (Fl) fluorite, (Cal) calcite, (Chl) chlorite, (Rhs) rhodocrosite, (Rdn) rhodonite, (Bst) bustamite, (Py) pyrite, (Ccp) chalcopyrite, (Mag) magnetite, (Bn) bornite, (Cct) chalcocite, (Cv) covellite, (Tnt) tennantite, (Fam) famatinite, (Eng) enargite, (Bno) bournonite, (El) electrum, (Au) native gold, (Ttr) tetrahedrite, (Sp) sphalerite, (Gn) galena, (Cstb) chalcostibenite, (Slm) seligmanite, (Grn) greenockite, (Hem) hematite, (Gth) goethite.

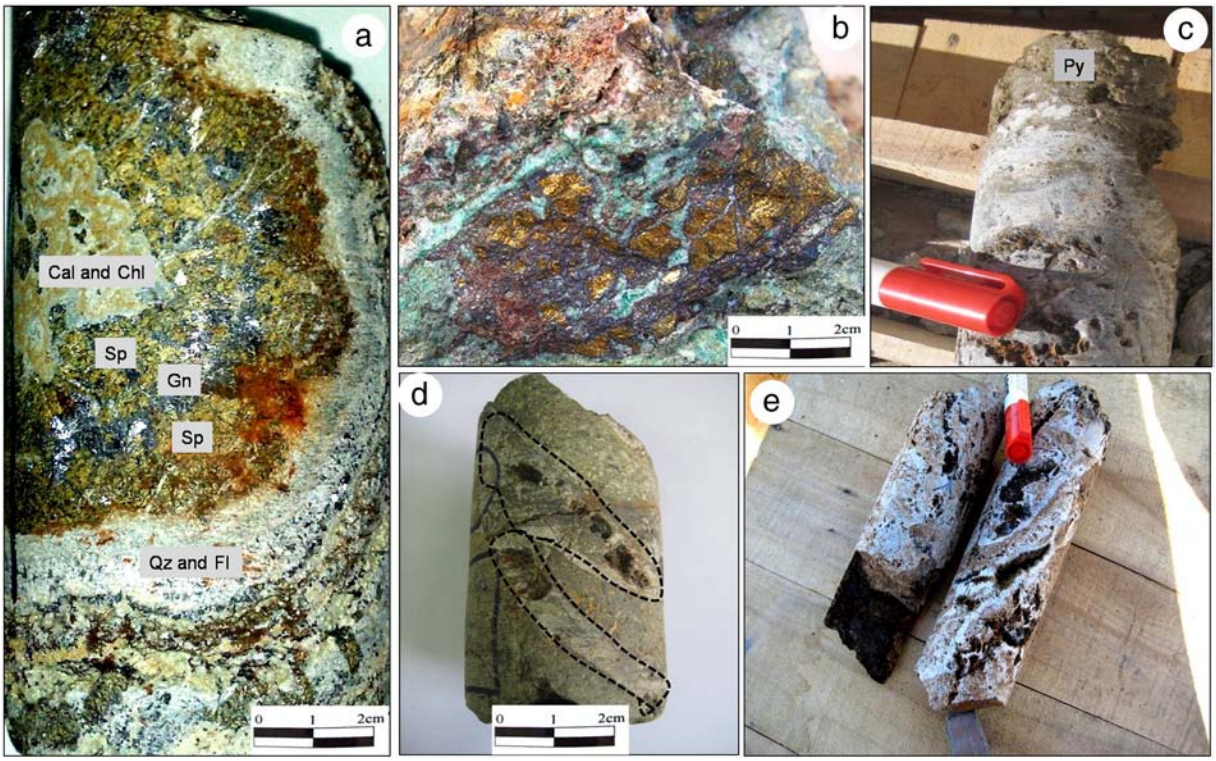

Fig. 5. Photographs of the different ore styles in the Glojeh mineralization veins: a) crustiform banding nearly symmetrical in sub-stage 2A; b) patches of chalcopyrite and bornite as breccia lenses and replacements; c) massive pyrite, magnetite, and silica bodies; d) veins and veinlets in sub-stage 2B; and e) precious metal-bearing hematite-quartz veins.

assemblage as breccias, massive ores, and replacement bodies (Fig. 5b). Chalcopyrite occurs as subhedral grains and is associated with bornite and chalcocite as fracture fillings (Fig. 6b). In some places, bornite is present as subhedral to anhedral grains adjacent to chalcopyrite. Enargite is associated with famatinite, chalcocite, covellite, bournonite, and pyrite, which are deposited surrounding chalcopyrite (Fig. 6c). Hematite is present in tabular shape and hosts gold grains (Fig. 6d), whereas sulfide minerals in this stage lack gold. Medium-grained quartz is associated with fluorite in the gangue in early stage.

Stage 2 is subdivided into three sub-stages, and characterized by Pb-Zn-Cu ± (Ag ± Cd) sulfide mineralization. Sub-stage 2A is characterized by the deposition of alternating veins, with symmetrical crustiform banded type texture (Fig. 5a), which was caused by initial deposition of coarse-grained quartz and fluorite, then followed by deposition of coarse-grained sphalerite, galena, and chalcopyrite as intergrowths or inclusions. Calcite, quartz, and sericite were deposited in the center of bands at the end of vein growth. Sphalerite occurs mostly as subhedral to anhedral crystals adjacent to galena and chalcopyrite (Figs. 6e, 7a), and as micro-inclusions in galena and chalcopyrite. It is characterized by green, white, honey yellow, and brown internal reflections under crossed nicols. Sub-stage 2B is characterized by deposition of fine-grained quartz, galena, and sphalerite veins and veinlets (Fig. 5d). These sulfosalt-rich veins and veinlets cut the sulfides deposited in sub-stage 2A (Fig. 6f). Minerals such as greenockite (Fig. 7b), argentite (Fig. 7c), zincian-tetrahedrite (Fig. 7d), argentian-tetrahedrite, tetrahedrite, chalcostibite ($CuSbS_2$), seligmanite, and tennantite (Fig. 6g) are present as major inclusions in galena. A submicroscopic intergrowth of native silver and argentite was detected during electron-microprobe analysis (Fig. 7c). Quartz and chlorite are the main gangue minerals in this sub-stage. Sub-stage 2C is characterized by the deposition of thin veinlets of galena, sphalerite, Mn-bearing silicate, and carbonates in association with quartz and calcite (Fig. 6h). Galena and sphalerite are the major sulfide minerals in this sub-stage. The Mn-bearing minerals include the silicates rhodonite ($MnSiO_3$) and bustamite ($CaMnSiO_3$) and the carbonate rhodocrosite ($Mn\,[CO_3]_2$).

Stage 3 is characterized by deposition of precious metals in quartz veins associated with hematite in vug infillings (Fig. 5e). It can be subdivided into two sub-stages. Sub-stage 3A is characterized by a wide variety of precious and sulfosalt minerals, which don't show a distinct paragenetic sequence. In order of decreasing abundance, the minerals are matildite, galenobismuthinite, Au–Ag alloy, native silver, native gold, meneghinite, polybasite, marrite, and aikinite (Figs. 6i, 7e to i). These minerals are typically abundant as inclusions in hematite. Sub-stage 3B is characterized by deposition of hematite in surface levels without any mineral inclusions. The hematite veins are altered to goethite due to supergene alteration, which is an important exploration guide.

4.3. Mineral chemistry

Stage 1: Pyrite composition (sub-stage 1A) is constant, with between 47.0% and 47.5% Fe, and with traces of arsenic. Gold content in pyrite is low and about 0.01 wt.% (Table 2). Chalcopyrite of sub-stage 1B contains 0.1–0.9 wt.% As. The composition of enargite and famatinite are close to being stoichiometric, although small amounts of Sb are present in enargite (0.1–0.8 wt.%).

Stage 2: The iron content of sphalerite (sub-stage 2A) is generally low (0.1–1.0 wt.%), except in sphalerite with 'chalcopyrite disease' (Bente and Doring, 1993, 1995; Barton and Bethke, 1987), which is mainly in the deeper parts of the veins with as much as 3.10 wt.% Fe. The sphalerite mostly contains 0.1 to 0.95 wt.% Cd, although one sample contained 2.4 wt.% Cd. Chalcopyrite, associated with galena and sphalerite and also in inclusions in sphalerite and galena in sub-stage 2A, has a composition close to stoichiometric. Galena tends to contain 0.01 to 1.2 wt.% As, with grains in shallower levels of veins having low contents (<0.1 wt.% As) than those in deeper levels (0.5–1.2 wt.% As). In sub-stage 2B, iron contents of sphalerite (<0.1 wt.%) are less than those in sub-stage 2A. The tennantite is rich in cooper (averages 41.82 wt.% Cu). The silver content in tetrahedrite (6.6 wt.% Ag) reflects the associated minerals, however argentian-tetrahedrite is closely associated

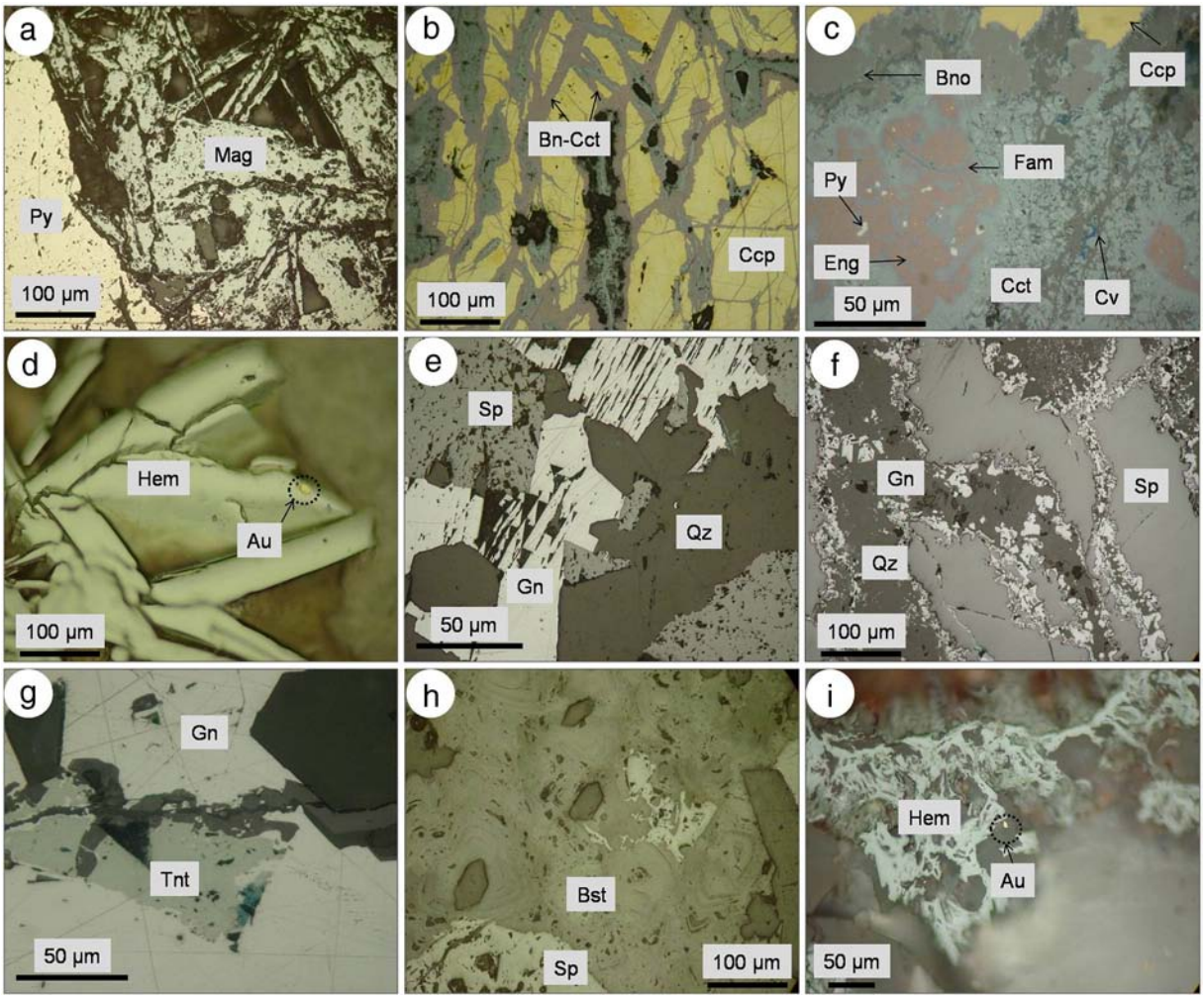

Fig. 6. Reflected light photomicrographs of ore mineral relationships: a) massive pyrite and magnetite (sub-stage 1A); b and c) Cu sulfide minerals (sub-stage 1B); d) gold inclusion in hematite (sub-stage 1A); e) sphalerite and galena (sub-stage 2A); f) veinlets of galena and sphalerite associted with inclusions of Ag-Cd-Sb bearing mineral; g) tennantite inclusion in galena (sub-stage 2B); h) sphalerite associated with Mn bearing carbonate and silicate, and i) gold mineralizationin in late stage. For abbreviations, see Fig. 4.

with argentite, with a content of 15.6 wt.% Ag. The high silver content of this sub-stage particularly characterizes the North Glojeh veins (average grade of 420 g/t Ag). The content of Se in the silver-bearing minerals is very low, as is common in many intermediate sulfidation epithermal deposits (Simon et al., 1997). Finally, iron content in sphalerite (sub-stage 2C) is very low (<0.1 wt.% Fe.). The composition of galena is close to stoichiometric.

Stage 3: The relative volumes of hematite, and their Au and Ag contents, confirm that hematite precipitation controlled the main Au-concentrating event in the Glojeh deposit (e.g., Ghasemi Siani, 2014). The Au/Ag ratio for this stage is ~0.50, which is almost three times more than the deposit average of ~0.16. Gold–Ag alloys occur as inclusions in hematite, with diameters from 10 to 60 μm and a composition that varies from 10 to 45 wt.% Ag. The selenium content is <0.05 wt.%. Native gold occurs as free grains in grey quartz and as inclusions in hematite. It contains 6.4 to 8.2 wt.% Ag. The bismuth-bearing minerals at the Glojeh are represented by matildite, native bismuth, galenobismuthinite, and aikinite (Table 2). Matildite is the most common and averages 1.01 wt.% Pb and 4.0 wt.% As. The galenobismuthinite contains 4.0 to 6.1 wt.% Ag. Polybasite is also a silver-carrier in the Glojeh sub-stage 3A mineralization. It occurs with meneghinite as small (as fine as 4 μm) inclusions in hematite. Polybasite also contains 30.3 wt.% Ag and 30.0 wt.% Sb (Table 2). The copper content is high (20.0 wt.% Cu), which is in accordance with the hypothesis of Bindi et al. (2007a, 2007b) that the copper content of pearceite-polybasite group minerals can be very high if selenium and (or) tellurium are not present. Meneghinite contains 37.35 wt.% Pb, 22.45 wt.% Sb and 18.1 wt.% Cu. Marrite contains 33.28 wt.% Pb, and 36.21 wt.% Ag, and aikinite contains 34.25 wt.% Pb and 34.65 wt.% Bi.

4.4. Hydrothermal alteration

Hydrothermal alteration zones are well-developed and zoned surrounding the Glojeh veins for ≈30 m within the host rocks (Fig. 8a). Laterally outward from the orebodies, there are four alteration assemblages including a silicic zone, a low-intermediate intensity quartz-sericite-pyrite (QSP) zone, an argillic zone, and a propylitic zone.

There are some different alteration characteristics between the North and the South Glojeh areas, which reflect the different host lithologies. The best-developed silicic alteration surrounds the North Glojeh rocks, such that outcrops and underground host rocks are totally silicified. On the other hand, propylitic alteration is much better developed in the South Glojeh area because of the more andesitic basalt wallrocks. Gemmel (2006) argued that in mafic rock-hosted epithermal systems, distal propylitic alteration is better developed than in felsic rock-hosted systems. In the argillic alteration zone, kaolinite and alunite are abundant in North Glojeh, whereas in South Glojeh, montmorillonite, illite, and chlorite are dominant. In general, overall alteration haloes in the South Glojeh area are more developed and better zoned than in North Glojeh.

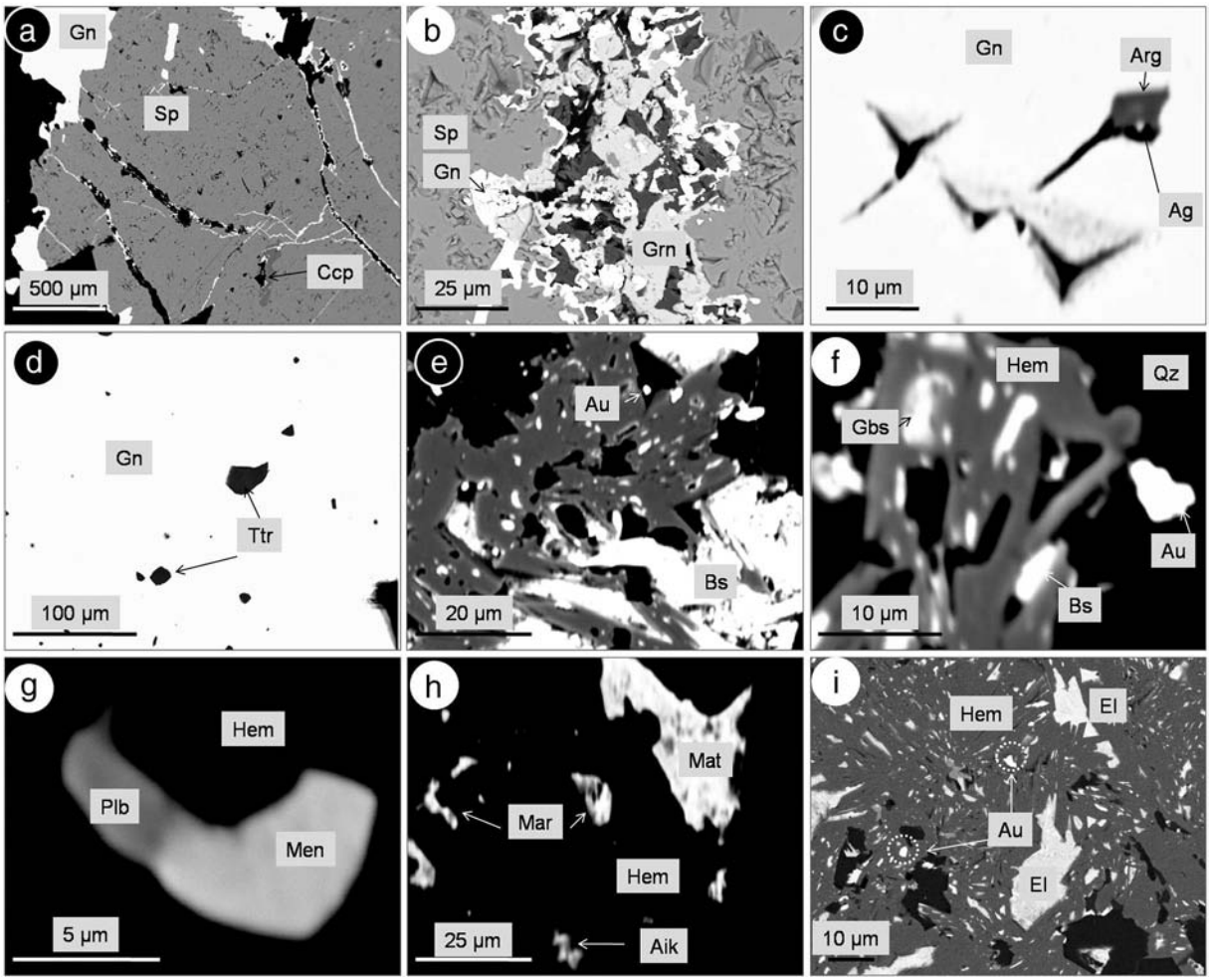

Fig. 7. SEM and EPMA photomicrograph of the Glojeh ore assemblages: a) sphalerite-galena and chalcopyrite of sub-stage 2A; b) inclusions of greenockite in galena (sub-stage 2B); c and e) sulfosalts in galena (sub-stage 2B), and e-i) precious metals and Ag-Bi-Sb bearing minerals associated with hematite in sub-stage 3A. For abbreviations, see Fig. 4, and other abbreviations include: (Arg) argentite, (Ag) native silver, (Mar) marrite, (Gbs) galenobismuthite, (Plb) polybasite, (Men) meneghinite, (Bs) bismuthinite, (Mat) matildite, (Aik) aikinite.

Silicification is represented by massive and vuggy silica bodies of quartz (Fig. 8b), anatase, chalcedony, and minor pyrite. The surrounding QSP alteration zone commonly consists of sericite or muscovite, quartz, pyrite, and minor calcite (Fig. 8c, e). Argillic alteration (Fig. 8d) led to the crystallization of quartz, kaolinite, alunite, montmorillonite, illite, chlorite, and pyrite, and the bleaching of the mafic lithology. In general, argillization is best marked by the complete replacement of plagioclase and K-feldspar by minerals such as montmorillonite, illite, and chlorite (Fig. 8f). Argillic alteration initially was characterized by formation of kaolinite-quartz and alunite (Fig. 8h), and was followed by montmorillonite-illite and particularly chlorite (Fig. 8i). Propylitic alteration is the most widespread alteration zone, particularly in the South Glojeh area, and consists of carbonate, epidote, chlorite, and minor jarosite, natrojarosite, and albite that were detected by XRD (Fig. 8g).

5. Analytical methods

Field work and sample collection in the Glojeh district was carried out between August 2011 and September 2012. A total of 178 polished and thin sections from mineralized veins and alteration zones were studied by optical microscopy. Suitable sections were selected for more study by FEI Quanta 650 FEG-ESEM and Zeiss 1450vp SEM, at the Leeds University and at the Iranian Mineral Processing Research Center (IMPRC), respectively. The SEM-EDS analyses and secondary electron (SEM-SE) images at the IMPRC were acquired using beam currents between 0.05 and 5 nA, and electron acceleration potentials of 5 to 20 kV.

Electron microprobe analysis of sections from the Glojeh vein samples was carried out using a Cameca SX100 at the IMPRC. The Cameca PAP correction software was used for data reduction. Backscattered electron images were used in order to select analytical points. Minerals were analyzed for Ag, As, Au, Bi, Cd, Cu, Fe, Pb, S, Sb, Se, Sn, Te, W, and Zn concentrations. Operating conditions were: 20 kV and 20 nA, with a beam diameter < 1 μm.

Thirty doubly polished sections of quartz, fluorite, and sphalerite from mineralized veins were prepared for fluid inclusion study. Microthermometric measurements were made on 460 primary inclusions, representing three stages of mineralization. Microthermometric measurements were performed at the University of Kharazmi, Iran, using a Linkam THM 600 freezing-heating stage, mounted on a ZEISS Axioplan2 research microscope. The precision of the temperature measurements was less than ±1 °C for heating and ±0.3 °C for freezing. Salinities in wt.% NaCl eq. and pressures in bars were calculated using FLINCOR version 1.4 (Brown, 1989) and FLUIDS (Bakker, 2003).

Isotopic analyses were conducted at the USGS stable isotope lab in Denver, CO. Separates of sphalerite, pyrite, chalcopyrite, and galena were combusted and analyzed for $\delta^{34}S$ according to the methods of Giesemann et al. (1994) using a CE Elantech Inc. Flash 2000 Elemental Analyzer coupled to a Thermo Finnigan Delta Plus XP ™ continuous flow mass spectrometer. All sulfide samples were analyzed with

Table 2
Summary of electron microprobe results for opaque minerals from the Glojeh epithermal deposit, data in wt.%. n.d: not analyzed, (n): number of analyses: 1) shallow sphalerite (sub-stage 2A); 2) deep sphalerite (sub-stage 2A); 3) deep galena (sub-stage 2A); 4) shallow galena (sub-stage 2A); 5) galena (sub-stage 2B); 6) sphalerite (sub-stage 2B); 7) chalcopyrite (sub-stage 1B); 8) chalcocite; 9) covellite; 10) enargite; 11) famatinite; 12) Zn-tetrahedrite; 13) tetrahedrite; 14) tennantite; 15) greenockite; 16) meneghinite; 17) bismuthinite; 18) electrum; 19) native gold; 20) pyrite (sub-stage 1A); 21) polybasite; 22) pyrite (sub-stage 1B); 23) matildite; 24) galenobismuthinite; 25) marrite; 26) aikinite.

	1(10)	2(8)	3(10)	4(10)	5(3)	6(5)	7(5)	8(2)	9(2)	10(6)	11(2)	12(2)	13(1)
S	33.37	33.30	10.55	10.87	10.75	33.32	33.45	21.20	31.30	28.70	27.60	26.21	27.84
Fe	0.10	0.75	0.01	0.01	0.01	0.08	32.71	0.10	0.10	0.16	0.25	0.80	1.20
Cu	0.00	0.01	0.01	0.03	0.01	0.00	32.75	77.80	66.80	50.20	43.26	27.20	29.70
Zn	64.20	65.65	0.10	0.12	0.10	66.21	0.00	0.00	0.00	1.20	0.01	1.83	3.24
As	0.20	0.00	0.75	0.04	0.01	0.00	0.46	0.20	0.20	16.40	0.54	0.65	0.55
Se	0.00	0.00	0.00	0.00	0.00	0.00	0.00	0.00	0.00	0.00	0.00	0.00	0.00
Ag	0.01	0.02	0.01	0.00	0.00	0.00	0.03	0.01	0.20	0.30	0.20	15.60	6.60
Cd	0.80	0.15	0.01	0.30	0.01	0.10	0.00	0.02	0.00	0.50	0.00	n.d	n.d
Au	n.d	n.d	n.d	n.d	n.d	n.d	0.02	0.00	0.00	0.01	0.00	n.d	n.d
Pb	0.00	0.00	88.60	86.90	88.75	0.00	0.00	n.d	n.d	n.d	n.d	n.d	n.d
Sb	0.01	0.03	0.01	0.01	0.00	0.00	0.01	n.d	n.d	0.50	28.20	27.60	30.10
W	0.01	0.01	0.00	0.00	0.00	n.d	0.02	n.d	n.d	n.d	n.d	n.d	n.d
Te	0.00	0.04	0.00	0.02	0.00	n.d	0.00	0.03	0.02	0.02	0.01	0.01	0.02
Bi	0.00	0.00	0.00	0.00	0.00	n.d	0.00	n.d	n.d	0.00	n.d	0.00	n.d
Sn	0.00	0.00	0.03	0.02	0.00	n.d	0.00	n.d	n.d	0.80	0.00	n.d	n.d
Total	98.70	99.96	100.08	98.32	99.64	99.71	99.45	99.36	98.62	98.79	100.07	99.90	99.25

	14(2)	15(15)	16(5)	17(2)	18(15)	19(3)	20(15)	21(2)	22(5)	23(3)	24(2)	25(2)	26(4)
S	26.40	21.20	19.10	24.30	0.00	0.00	53.00	18.00	53.50	17.50	23.10	16.00	19.35
Fe	4.80	0.01	0.01	n.d	0.00	0.13	47.10	0.00	47.26	0.30	0.04	0.01	0.01
Cu	41.82	0.00	18.10	1.40	0.01	0.01	0.02	20.00	0.10	0.01	0.00	0.10	9.60
Zn	0.00	0.61	0.00	n.d	0.00	0.03	0.02	0.00	0.00	n.d	0.00	0.00	0.01
As	12.30	0.02	0.00	0.01	n.d	n.d	0. 10	0.10	1.00	4.00	0.30	12.20	0.15
Se	0.01	0.01	0.00	0.00	0.01	n.d	0.00	0.00	0.00	0.00	0.02	0.00	0.00
Ag	1.00	0.41	0.08	0.00	25.00	7.50	0.01	30.30	0.01	23.65	5.50	36.21	0.00
Cd	0.00	75.50	0.00	n.d	0.01	0.01	n.d	0.80	n.d	n.d	n.d	n.d	0.00
Au	0.00	0.00	0.00	n.d	72.50	92.00	0.01	0.00	0.02	0.00	0.00	0.00	0.00
Pb	n.d	0.20	37.35	1.03	n.d	n.d	n.d	0.00	n.d	1.01	36.40	33.28	34.25
Sb	13.41	0.00	22.45	0.00	n.d	n.d	0.00	30.00	0.01	0.00	0.00	0.00	0.00
W	n.d	0.00	0.00	n.d	n.d	n.d	0.01	n.d	0.00	n.d	n.d	n.d	0.01
Te	0.00	0.00	0.00	0.00	0.00	0.00	0.01	0.00	0.02	n.d	n.d	n.d	0.01
Bi	n.d	0.00	0.15	73.12	n.d	0.16	n.d	0.00	n.d	53.25	35.50	0.00	34.65
Sn	n.d	0.00	n.d	0.00	n.d	n.d	n.d	n.d	n.d	n.d	n.d	n.d	n.d
Total	99.74	97.96	97.24	99.86	97.53	99.84	100.28	99.20	101.92	99.72	98.86	97.80	98.04

nationally accepted standards NBS123 + 17.44 per mil and IAEA-S-3 −32.55 ± 0.12 per mil (Coplen et al., 2002). Values of $\delta^{34}S$ are expressed relative to Vienna Cañon Diablo Troilite (VCDT) with a precision of 0.2‰. Oxygen isotope analysis of handpicked quartz closely follows the procedure described by Clayton and Mayeda (1963) with the extraction of oxygen from quartz in a BrF5 extraction line. The resulting CO_2 gases were measured using a Finnigan MAT 252 mass spectrometer and the results are expressed in $\delta^{18}O$ relative to VSMOW with a precision of 0.2‰.

6. Fluid inclusion studies

Quartz, fluorite, and sphalerite samples, representative of all three hydrothermal stages, were collected from drill-core covering much of the Glojeh district. Fluid inclusions suitable for study generally ranged from 10 to 25 μm in length, although a few were as large as 45 μm across (Fig. 9). These inclusions vary in shape from negative crystal, elongate, rounded, and to irregular. Two-phase, liquid-rich inclusions containing approximately 80 to 85% liquid and 15 to 20% vapor and two-phase vapor-rich inclusions containing >95% vapor and <5% liquid were the only identified inclusions.

Coexisting liquid-rich and vapor-rich inclusions (Fig. 9) were observed in some of the samples, which could indicate boiling conditions at the time of trapping. Homogenization and melting temperatures were generally not measured for vapor-rich inclusions due to the difficult nature of observing phase changes in cavities with negligible amounts of liquid. However, a couple of vapor-rich inclusions were homogenized into the vapor phase and they gave temperatures consistent with the adjacent liquid-dominated inclusions.

Microthermometric data for Glojeh are presented in Table 3 and Figs. 10 and 11. Homogenization temperatures determined from primary inclusions in samples from the North Glojeh veins range from 170 to 340 °C. Salinities range from 0.5 to 11.0 wt.% NaCl eq. based upon ice melting temperatures of −7.2 to −0.4 °C. For the South Glojeh vein samples, homogenization temperatures are 150 to 320 °C and salinities are 0.1 to 10.1 wt.% NaCl eq. based on ice melting from −6.6 to −0.1 °C. Fluid inclusion measurements in samples from both areas thus show similar characteristics.

Recognition of fluid inclusions trapped under conditions of boiling or immiscibility is valuable for P-T estimations because the homogenization temperatures equal the trapping temperatures (Roedder and Bodnar, 1980), which eliminates the need for a pressure correction to obtain the trapping temperature. The two populations of fluid inclusions, liquid-rich and vapor-rich, observed in the Glojeh system homogenize to liquid and vapor, respectively, within the same temperature range, suggesting entrapment under boiling conditions. Additionally, the presence of chalcedony and colloform quartz may indicate boiling (Hedenquist et al., 2000; White and Hedenquist, 1990). The calculated pressures of fluid inclusions from stage 1, 2, and 3 are 90, 36, and 10 bars, respectively, and densities of fluid inclusions range from 0.8 to 0.9 g/cm^3.

The stage 1 assemblage was deposited from solutions with 5 to 11 wt.% NaCl eq. salinity at temperatures of 220 to 340°, whereas base-metal sulfides deposited (stage 2) were precipitated from solutions with 1 to 8 wt.% NaCl eq. salinity at temperatures of 200 to 290 °C. The precious metal mineralization (stage 3) was deposited from solutions of 0.1 to 2 wt.% NaCl eq. salinity at temperatures <200 °C.

The relationship between homogenization temperature and salinity of the fluid inclusions (Fig. 12) is characteristic of boiling, isothermal

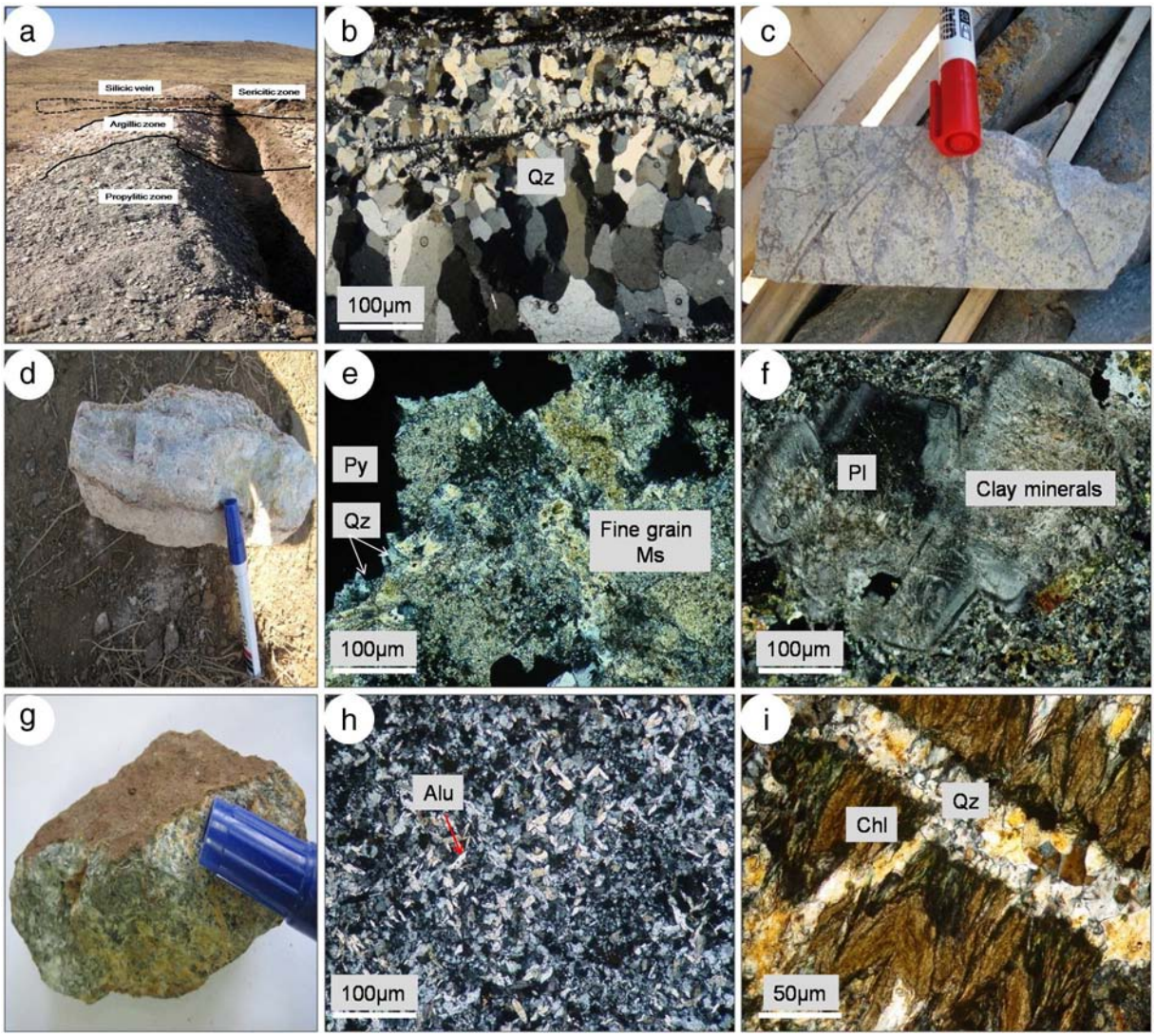

Fig. 8. Photomicrographs of alteration types in the Glojeh district: a) show that zoning of alteration types surrounding South Glojeh veins; b) crustiform quartz in silicic zone; c and d) hand samples of sericitic and argillic zones, respectively; e) quartz, pyrite, fine-grain muscovite, and minor calcite in sericitic alteration; f) plagioclase phenocrysts replaced by clay minerals (montmorillonite and illite) in argillic zone; g) hand samples from propylitic zone; h) subhedral alunite in argillic zone, and i) argillic zone rich in chlorite. Other abbreviations: (Pl) plagioclase, (Ms) muscovite, and (Alu) alunite.

mixing, and dilution of hydrothermal fluids during the different mineralization stages as described by Wilkinson (2001). These fluid inclusion data correspond to a shallow event caused by a low temperature fluid (stage 3), an intermediate sulfidation stage event represented by the stage 2 base metal-rich assemblage, and a deeper high sulfidation stage in the veins (stage 1). The data show a positive correlation between homogenization temperature, salinity, and depth. In order to obtain mineralization depth for Glojeh, the temperature-depth diagram (Haas, 1971) was used in this study. According to Haas (1971), it is possible to estimate the maximum depth below the water table of mineralization if evidence of boiling is provided. Based on such boiling evidence (Figs. 9 and 12), it can be estimated that stages 1 to 3 formed at depths of 1100 m, through 500 m, and to 380 m, respectively.

7. Stable isotopes

The $\delta^{18}O$ value for most quartz from the three stages is in the range of 11.2 to 13.3‰, with one anomalously low value of 8.8‰ for late stage quartz from the South Glojeh area (Table 4). The calculated $\delta^{18}O$ range of the fluids in equilibrium with stages 1 and 2 quartz is about 4–8‰, when using the relationship of Meheut et al. (2007) and at temperatures obtained from fluid inclusions of 250–300 °C. The data show little difference between the North Glojeh and the South Glojeh veins. The one sample with the anomalously low quartz measurement is for stage 3 quartz and has a calculated fluid value of about 0‰.

Oxygen isotope values for vein quartz and estimated oxygen values for the ore fluids are similar to those of epithermal deposits in many volcano-plutonic environments (Vallance et al., 2004; Vallance et al., 2003). The lack of hydrogen isotope values and lack of knowledge of the isotopic composition of meteoric fluid in this region at the time of mineralization prevent us from defining with certainty the fluid sources. Nevertheless, the stage 1 and 2 oxygen isotope values are very consistent with a magmatic water source, although one can never fully rule out interaction of meteoric fluid with surrounding volcanic wall rocks under very low water-rock conditions. The very low fluid value for the stage 3 quartz clearly indicates the importance of meteoric water in the late-stage mineralizing event. Whether such a late-stage fluid was entirely of meteoric origin and shifted to higher $\delta^{18}O$ during wallrock interaction, or whether there was some mixing of the meteoric water with a late stage magmatic fluid is uncertain.

Sulfur isotope values were measured for 13 samples of sphalerite, pyrite, chalcopyrite, and galena, which were selected from two stages

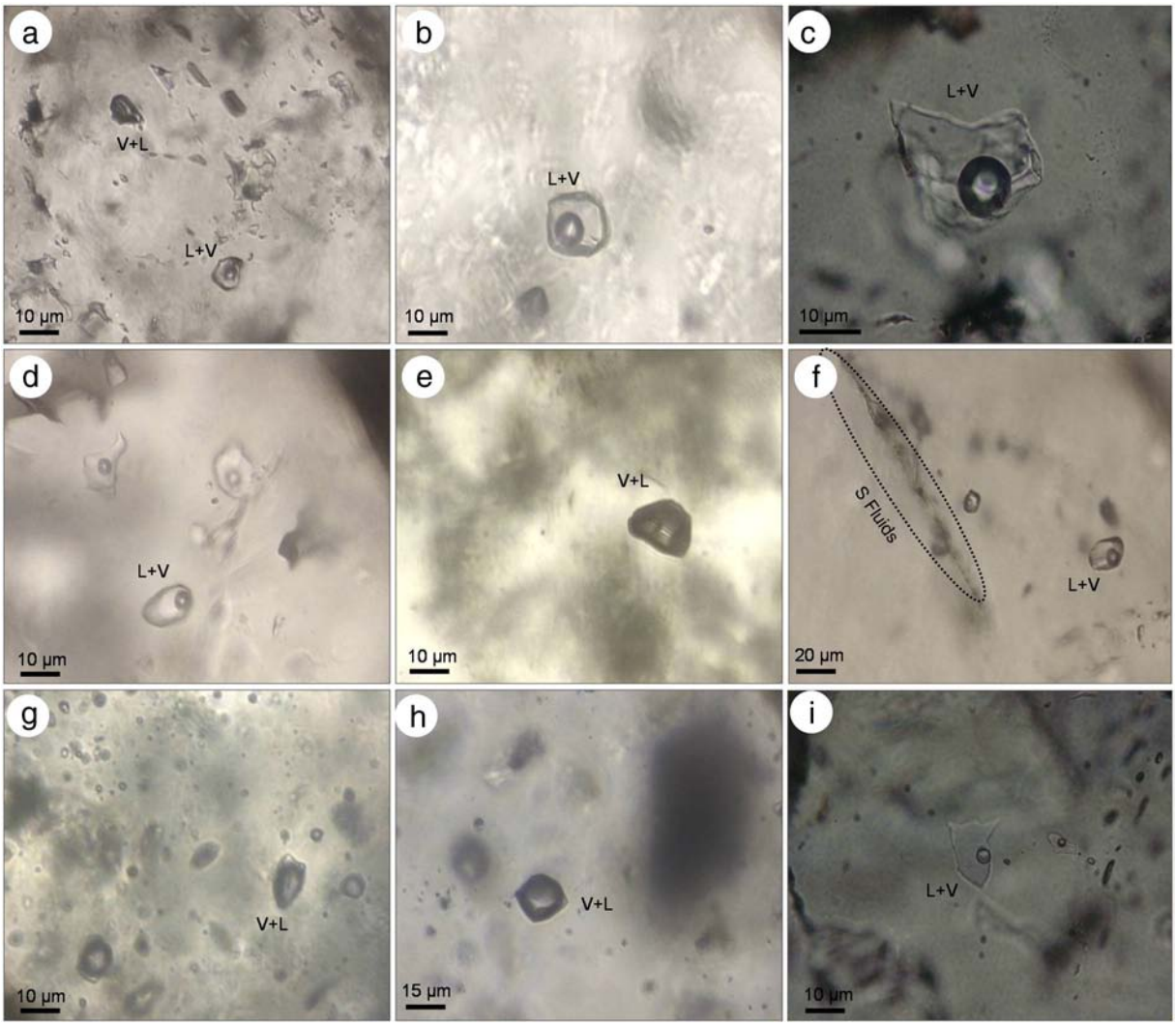

Fig. 9. Photomicrographs of fluid inclusions in Glojeh veins: a) coexisting liquid-rich and vapor-rich fluid inclusions in quartz (sub-stage 1A); b) primary fluid inclusions in fluorite (sub-stage 1B); c) primary fluid inclusions in quartz (sub-stage 2A); d) primary fluid inclusions in quartz (sub-stage 1B); e) vapor-rich fluid inclusions in sphalerite (sub-stage 2A); f) primary and secondary fluid inclusions in quartz (sub-stage 2C); g and h) vapor-rich fluid inclusions in quartz (sub-stage 1B), and i) primary fluid inclusions in quartz (sub-stage 2B).

of mineralization (Table 4). The measured $\delta^{34}S$ for the sulfide minerals are mostly between −7.3‰ and +1.3‰ for stages 1 and 2 in the North Glojeh area, and −0.3‰ and +8.4‰ for stages 1 and 2 in the South Glojeh area. These data might suggest a different sulfur source in the two mineralized areas, despite similar fluid inclusion characteristics and oxygen isotope measurements. Assuming the rhyodacite and andesitic basalt in the two parts of the district have different sources, it is possible that the ore fluids in the two areas were exsolved from two different magmas with different sulfur isotope compositions. Two distinct fluids could help explain differences in the metal assemblages in the two areas. Nevertheless, particularly as fluid inclusion and oxygen isotope data are consistent between the two areas, the variation in $\delta^{34}S$ could indicate a single sulfur reservoir with variations due to changes in pH and fO_2 between the two areas. In either case, considering the volcanic nature of the host rocks at the Glojeh, sulfur in the ore fluids would be derived either directly from magmatic exsolution or by leaching of volcanic host rocks (e.g., Cooke and Simmons, 2000).

Table 3
Summary of fluid inclusions data: Homogenization temperature Th; Final ice melting temperature Tm_{ice}; Number of analyses (n).

Inclusion type	Host mineral	Mineralization stage	Type	Tm_{ice}°(C) North Glojeh	Th °(C) North Glojeh	Salinity wt.% NaCl eq North Glojeh	Tm_{ice}°(C) South Glojeh	Th °(C) South Glojeh	Salinity wt.% NaCl eq South Glojeh
L + V	Sphalerite (n = 7)	Stage 2	Primary	−3.6 to −4.3 (24)	200–250 (41)	5.9 to 7.0	−1.8 to −3.0 (25)	160–290 (47)	3.0 to 5.0
L + V	Quartz (n = 6)	Sub-stage 1B	Primary	−0.4 to −4.8 (65)	170–290 (55)	0.5 to 7.7	−1.5 to −3.0 (41)	160–290 (54)	2.5 to 5.0
L + V	Quartz (n = 6)	Stage 1B	Primary	−3.6 to −6.5 (31)	220–320 (43)	6.0 to 10.0	−2.4 to −6.6 (72)	220–300 (44)	4.0 to 10.1
L + V	Fluorite (n = 3)	Stage 1B	Primary	−6.0 to −7.2 (29)	230–320 (44)	9.4 to 11	−1.8 to −6.6 (51)	200–320 (46)	3.0 to 10.1
L + V	Quartz (n = 5)	Stage 3	Primary	−0.5 to −1.8 (16)	170–230 (30)	0.6 to 3.3	−0.1 to −1.2 (18)	150–190 (16)	0.1 to 2.0
L + V	Quartz (n = 3)	Stage 1A	Primary	−4.3 to −4.8 (17)	260–340 (39)	7.0 to 7.7	−3.6 to −4.8 (17)	270–290 (12)	6.0 to 7.7

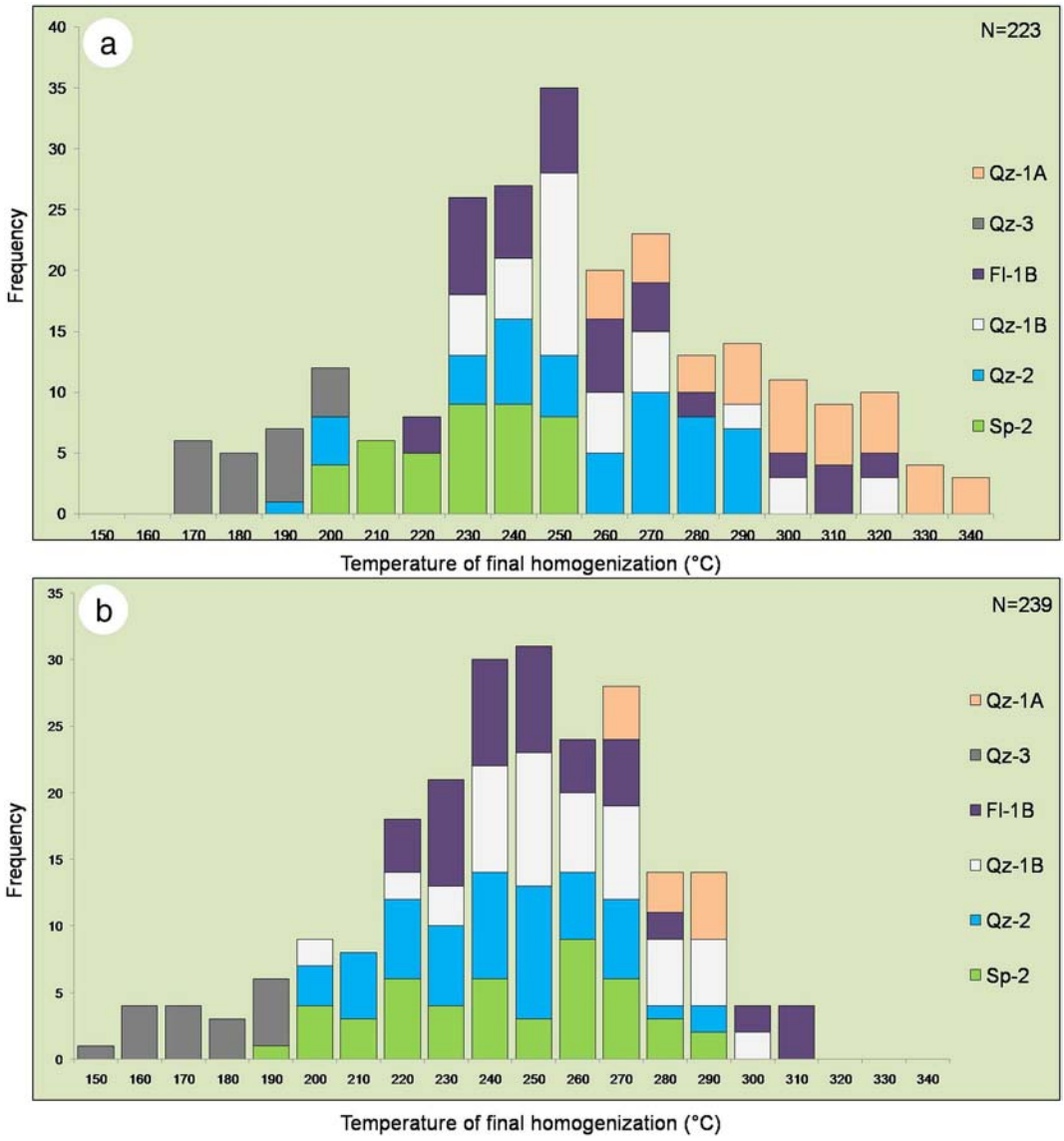

Fig. 10. Histograms of homogenization temperatures for primary inclusions in: a) the North Glojeh veins; b) the South Glojeh veins; Mineral abbreviations are as follows: sphalerite (Sp), quartz (Qz), fluorite (Fl). The numbers indicate the paragenetic stage.

8. Discussion

8.1. Timing of gold mineralization

The $^{40}Ar/^{39}Ar$ mineralization age for the North Glojeh and South Glojeh veins has been determined to be 42.20 ± 0.34 and 42.56 ± 1.47 Ma, respectively (Table 1). These ages, when considering the analytical uncertainty, are identical coeval at ~42 Ma, and are interpreted to represent the timing of gold mineralization.

The Goljin stock, with a plateau age of 41.87 ± 1.58 Ma, is contemporaneous with the mineralization age. Considering the close spatial association of the stock and the Glojeh epithermal mineralization, it may be inferred that the Goljin stock is genetically related to the mineralization. The ca. 39 Ma age for the Varmarziar stock appears to be young to be genetically related to the epithermal mineralization. Furthermore, the discovery of the Glojeh gold deposit provides us with important implications for exploration targeting of epithermal ores in the volcanic rocks, particularly close to granite and granodiorite stocks in the Tarom-Hashtjin metallogenic province and possibly in the Ahar-Arasbaran Belt. Whether or not economic porphyry mineralization could also be present is uncertain. As mentioned above (geology section), mineralization in the Glojeh area is related to magmatism that occurred during subduction of the Urmieh-Dokhtar island arc to the northwest beneath the Alborz-Azarbayejan micro-continent.

8.2. Source of mineralizing fluid

The origin of the hydrothermal fluids that form epithermal deposits can be varied; from predominantly magmatic in high sulfidation (HS) epithermal deposits to predominantly meteoric in low sulfidation (LS) deposits (Hedenquist et al., 2000; Cooke and Simmons, 2000; Hedenquist et al., 1998; Hedenquist et al., 1996; Arribas et al., 1995; Rye et al., 1992). Intermediate sulfidation (IS) deposits in general have a closer affiliation with HS deposits and porphyries than with LS deposits (Camprubí and Albinson, 2007; Sillitoe and Hedenquist, 2003; Sillitoe et al., 1998).

The salinity of fluid inclusions in the Glojeh defines a wide range from 0.1 to 11 wt.% NaCl eq., with the higher salinity measurements consistent with at least some of the fluid from a magmatic source. The narrow range of the measured $\delta^{18}O$ in quartz between 4 and 8‰ also is consistent with a dominantly magmatic fluid, although the lack of δD data prevents us from defining any significant contribution of

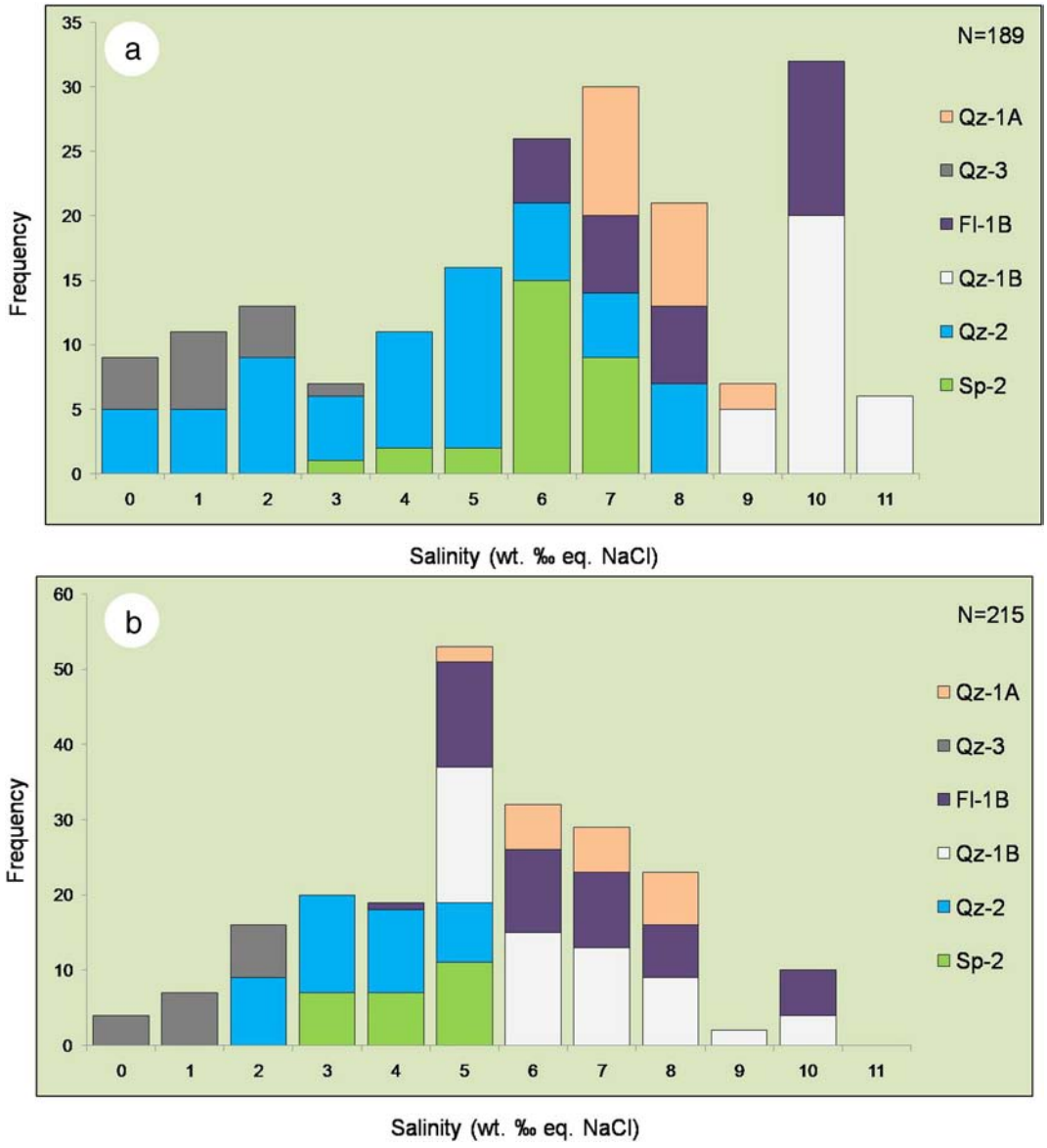

Fig. 11. Histograms of salinity for primary inclusions in: a) the North Glojeh veins; b) the South Glojeh veins; Abbreviations as in Fig. 10.

meteoric fluid in the Glojeh deposit. Three fluid groups include (a) moderate temperature and salinity (stage 1), with ranges of 220 to 340 °C and 5 to 11 wt.% NaCl eq., respectively; (b) slightly lower temperature fluid inclusions, homogenizing between 200 and 290 °C, with slightly lower salinities of 1 to 8 wt.% NaCl eq. (stage 2); and (c) low temperature and low salinity fluids (stage 3) (150–200 °C, 0.1 to 2 wt.% NaCl eq.). We interpret these data to reflect a magmatic hydrothermal fluid during stage 1, which may have mixed with some meteoric water during stage 2, and a much later event with dilution by meteoric water (stage 3). This interpretation is consistent with similar conclusions in other magmatic-hydrothermal systems, such as those described by Camprubí and Albinson (2007) for formation of IS epithermal deposits in Mexico. They too concluded that the heavy oxygen values, similar to what we have measured, reflect mainly magmatic fluid contributions.

The consistent $\delta^{34}S$ values of about 0‰ for the North Glojeh area are interpreted as the result of magmatic sulfur escaping from a crystallizing magma. However, the sulfur values for the South Glojeh area are significantly depleted. We suggest that they reflect either similar magmatic sulfur that has been modified by interaction with crustal rocks or fluid from a second magma source, but magma that itself has undergone some amount of crustal contamination.

8.3. Fluid evolution and mineral zoning

In a broad sense, mineralogy, mineralization age, and paragenesis in veins from both areas are similar, which suggests that they could have a common origin. Nonetheless, some important differences are observed both locally and on a regional scale. At the vein scale, stage 1 mineralization is present at deepest levels (200 to 300 m), and galena, sphalerite, and chalcopyrite (stage 2) are most abundant at shallower depths (50 to 200 m). Anomalous silver is associated with the shallower base metal assemblage, whereas gold concentrations (stage 3) are greatest at near surface levels. This pattern of zoning at the vein scale is consistent with the zoning pattern proposed by Buchanan (1981) for epithermal veins.

On a regional scale, there are other important zoning features. The North Glojeh veins are richer in silver and base metals, whereas the South Glojeh veins are more gold-rich. Although both vein groups have similar homogenization temperatures and salinities (i.e., 170–340 °C and 0.5 to 11 wt.% NaCl eq. for the North Glojeh and 150–320 °C and 0.1 to 10.1 wt.% NaCl eq. for the South Glojeh), as well as similar oxygen isotope compositions, they have notable differences in $\delta^{34}S$. This could indicate that the fluid sources for South Glojeh and North

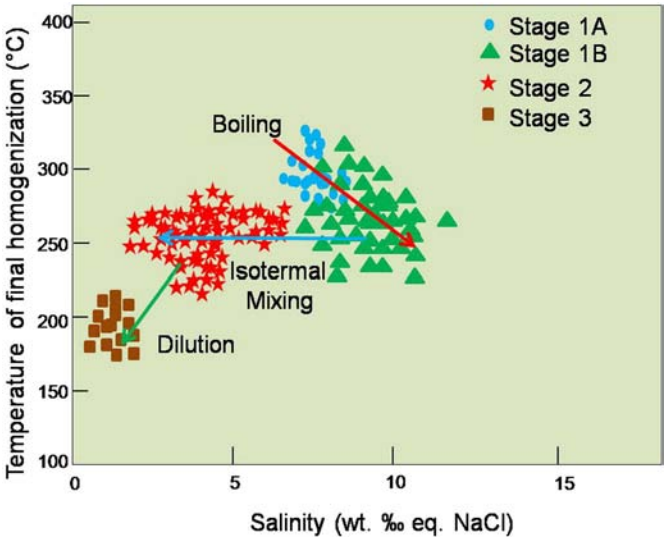

Fig. 12. Th vs. salinity plot for fluid inclusion data for the Glojeh veins showing boiling, isothermal mixing and dilution trend during mineralization based on Wilkinson (2001); red arrow shows boiling process, blue arrow shows isothermal mixing, and green arrow shows dilution by pure meteoric water.

Glojeh were different, as mentioned above, although $^{40}Ar/^{39}Ar$ age and paragenetic similarities between the veins of the two areas show that they are cogenetic and have generally similar metal signatures. If the veins were formed by the fluids with a common source, then the greater sulfur fugacity, slightly higher temperatures, more abundant silver and base metals, and greater salinities to the north could indicate that the North Glojeh veins are in closer proximity to the ultimate heat source.

8.4. Ore-bearing fluid composition

Sub-stage 1A is characterized by vuggy quartz and massive magnetite and pyrite. The iron-rich minerals are hosted largely by vuggy quartz in which there are no aluminosilicate minerals remaining. Vuggy quartz in this stage indicates that alteration was by a fluid with pH < 2 (Arribas, 1995).

Mineralization in sub-stage 1B commenced with deposition of chalcopyrite and bornite, which were then replaced by high sulfidation state minerals. Covellite, famatinite, and enargite, and their abundance suggest temperatures of ≤300 °C and high sulfur fugacity of the hydrothermal fluids (Einaudi et al., 2003). Initially hydrothermal fluids may have attained a very high sulfidation state (fS_2 of 10^{-8}–10^{-10} and fO_2 is 10^{-31}–10^{-33}) at temperatures near 300 °C, and if they were oxidized and silica-undersaturated, their high ratio of H_2S/Fe would have prevented deposition of Au with the Cu–Sb-As-Fe-rich sulfides (Williams-Jones and Heinrich, 2005). Both argillic and sericitic alteration assemblages are the product of an acidic fluid that mobilized alumina, and the presence of alunite suggests an acidic pH (Stoffregen, 1987).

Fluid conditions during the sub-stage 1B events would have fluctuated from the intermediate sulfidation state (chalcopyrite and bornite) to the high sulfidation state (covellite and enargite). Eventual decrease in sulfur fugacity and increase in oxygen fugacity, combined with a decrease in temperature to approximately 250 °C, would have caused the shift to deposition of hematite and gold. Gold in this sub-stage was deposited as inclusions in hematite. Fluid inclusion data indicate stage 1 salinities were in the range of 5 to 11 wt.% NaCl eq. and are similar to those of many high-sulfidation Au-Cu-As deposits (e.g., 6 to 13 wt.% NaCl eq. at Cerro Rico, Potosí: Steele, 1996).

The base metal assemblage of stage 2 is consistent with an intermediate sulfidation state hydrothermal system. Knowing fluid temperature and sphalerite composition, the fS_2 may be inferred using published experimental data (e.g., Czamanske, 1974; Scott and Kissin, 1973; Scott and Barnes, 1971; Barton and Toulmin, 1966). The average temperature of stage 2 is estimated as 245 °C from fluid inclusion studies. Because the XFeS is in the 0.1–1.0 mol% range in this stage, fS_2 is estimated between $10^{-10.0}$ and $10^{-11.5}$ bars. These values are consistent with the intermediate sulfidation field as illustrated in Einaudi et al. (2003). During stage 2, the Fe content of sphalerite decreased with time, reflecting increase in oxygen fugacity or decrease in sulfur fugacity. Based on the base metal- and silver-rich mineralization, sulfur fugacity, presence of Mn-bearing carbonates and silicates, temperature and salinities of fluid inclusions, sulfide and sulfosalt mineral assemblage, and low FeS content of sphalerite, stage 2 is consistent with an intermediate-sulfidation hydrothermal system. Intermediate-sulfidation deposits show a large range in metal compositions, as well as great variability in silver and gold concentrations (Albinson et al.,

Table 4
Oxygen and sulfur isotope data for quartz and sulfide minerals. $\delta^{18}O$ fluid values were calculated using the fractionation equation of Meheut et al. (2007), and $\delta^{34}S_{H2S}$ values were calculated using the fractionation equation of Ohmoto and Rye (1979). The temperatures for these calculations were based on fluid inclusion measurements.

Sample	Location	Mineralization stage*	T°C	$\delta^{18}O$ mineral‰	$\delta^{18}O_{fluid}$‰	$\delta^{34}S$ mineral‰	$\delta^{34}S$ H_2S‰
G392–14	North Glojeh	Quartz (1)	285	11.2	4.9		
G392–14 B	North Glojeh	Quartz (1)	285	11.2	4.9		
G392–17	North Glojeh	Quartz (1)	290	13.2	7.2		
G392–13	North Glojeh	Quartz (1)	300	13.2	7.6		
G392–13 B	North Glojeh	Quartz (1)	300	13.3	7.7		
G392–15	North Glojeh	Quartz (2)	260	11.6	4.1		
G392–12	South Glojeh	Quartz (3)	250	8.8	0.7		
G102	South Glojeh	Quartz (2)	268	12.9	5.9		
G392–16	North Glojeh	Quartz (2)	250	11.6	4.1		
G392–1	North Glojeh	Sphalerite (2)	250			−5.3	−5.9
G392–2	North Glojeh	Galena (2)	250			−6.8	−9.1
G392–3	North Glojeh	Sphalerite (2)	250			−4.4	−4.8
G392–4	North Glojeh	Galena (2)	250			−6.5	−8.8
G392–5	South Glojeh	Galena (2)	250			−0.3	−2.6
G392–6	North Glojeh	Galena (2)	250			−7.3	−9.6
G392–7	South Glojeh	Pyrite (1)	300			8.4	7.2
G392–8	South Glojeh	Chalcopyrite (1)	280			0.5	0.1
G392–9	South Glojeh	Galena (2)	250			0.7	−1.6
G392–10	South Glojeh	Sphalerite (2)	250			0.5	0.1
G392–11	North Glojeh	Pyrite (1)	300			1.3	0.1
G392–12	North Glojeh	Sphalerite (2)	250			−4.3	−4.7
G392–13	North Glojeh	Galena (2)	250			−7.3	−9.6

* Numbers in bracket are mineral assemblage stage.

2001). There is a consistent increase in salinity with increasing base metal content and Ag/Au ratio, as we observed in our stage 2 data. Sub-stage 2A, with abundant base metals, has a high salinity (6 to 8 wt.% NaCl eq.), relative to that (3 to 6 wt.% NaCl eq.) of silver-rich sub-stage 2B. Thus, there is a clear relationship between low salinities and low Ag/Au ratios, as well as low base metal contents (Henley, 1985, 1990; Hedenquist and Henley, 1985). Oxygen isotope values in stage 2 are lower than those of stage 1, suggesting that mixing between magmatic and meteoric fluids occurred during base metal mineralization.

Estimation of the $fS2$ associated with precious metal deposition in stage 3 at low temperature (≈160 °C), using the native bismuth-bismuthinite equilibrium, yields an $fS2$ of 10^{-14} bar. Stage 3 is major stage for gold precipitation. We speculate that stage 3 resulted from dilution of hydrothermal fluids by meteoric water.

This transition between the high- and intermediate-sulfidation types is well recognized (e.g., Einaudi et al., 2003; Sillitoe and Hedenquist, 2003; Sillitoe, 1999a; Margolis et al., 1991), with numerous district-scale observations, such as in the Julcani and Colquijirca districts of Peru, and the Pyramid district of Nevada. At Julcani and Pyramid, high-sulfidation enargite-bearing veins with alunite halos are transitional along strike to intermediate-sulfidation veins richer in Zn and bordered by sericitic alteration (Deen et al., 1994; Wallace, 1980).

8.5. Ore deposition model

The Th vs. salinity diagram (Fig. 12) shows the occurrence of three major processes of boiling, mixing, and dilution from the early stage to the late stage of mineralization. The sources of the mineralizing fluids and the proposed mechanisms of precipitation for the mineral associations at the Glojeh epithermal deposit are summarized in Fig. 13. The conceptual model is developed based on petrographic observations and fluid inclusion and stable isotope studies. Fluid inclusion and stable isotope data show the occurrence of two fluid types in all mineralization stages; magmatic and meteoric fluids (deep and shallow) to variable degrees. These results are comparable to those found in the study of several Mexican epithermal deposits (Velador, 2010; Albinson et al., 2001; Gemmell et al., 1988; Norman et al., 1997b). We conclude that higher salinities and temperatures of stage 1 fluids reflect their exsolution from a magmatic source, which could be related to unrecognized copper-gold porphyry mineralization at depth. High-salinity fluids related to porphyry copper mineralization are well documented in the literature (e.g., Beane and Titley, 1981) and are thought to have evolved from magmas (e.g., Velador, 2010; Pudack et al., 2009; Burnham, 1979; Henley and McNabb, 1978).

A fluid from a magmatic source at a relatively high temperature was responsible for the initial deposition of massive pyrite and magnetite (sub-stage 1A). The acidic character of the fluid, together with the

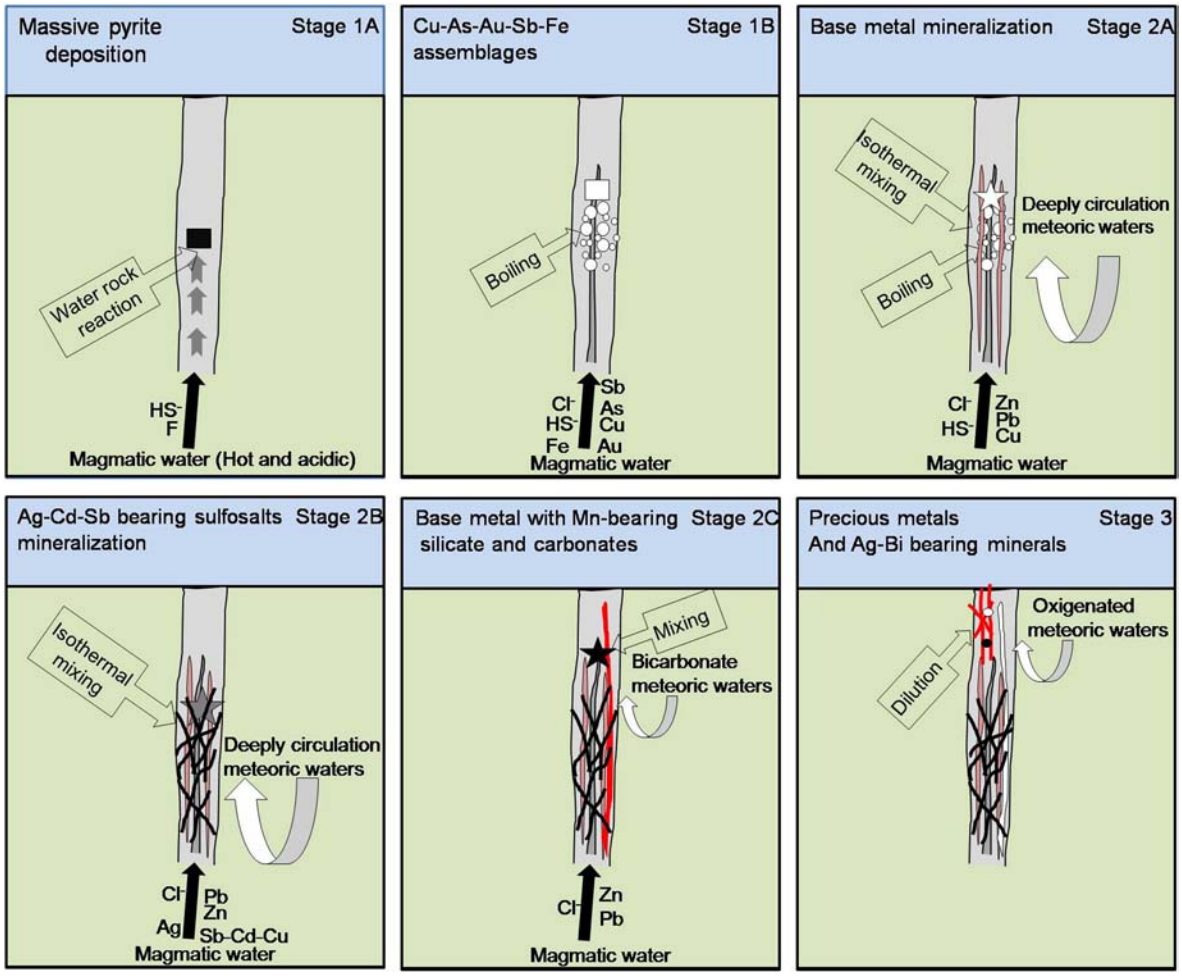

Fig. 13. Summary of the plausible precipitation mechanisms for mineralization at the Glojeh epithermal deposit, based upon paragenetic relations, and fluid inclusion and stable isotope analyses: Black square is related to massive pyrite and magnetite precipitation; white square is Cu-Au-As-Sb-Fe mineralization caused by boiling process; white star represents the base metal mineralization; black star is base metal mineralization associated with Mn-bearing silicate and carbonates; gray star represent the occurrence of sulfosalt inclusions in galena; black circle represent the occurrence of precious metal mineralization; and white circle represent the occurrence of barren oxy-hydroxides.

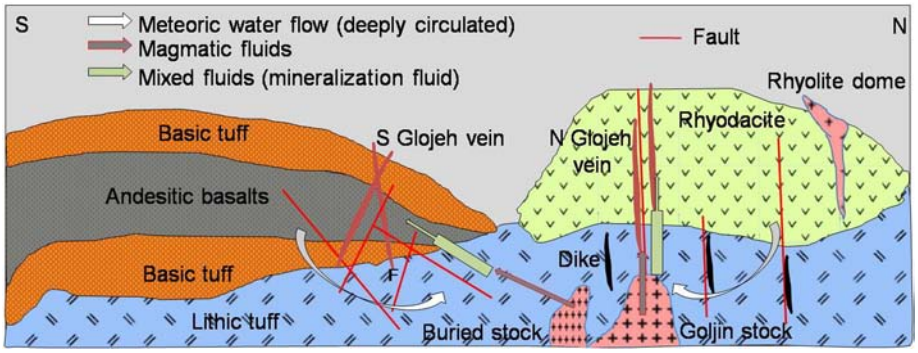

Fig. 14. Schematic genetic model for the Glojeh district: The model shows magmatic fluids derived from an intrusion (Goljin intrusion, or an unidentified coeval intrusion) that mix with deeply circulating meteoric water, forming the North Glojeh and South Glojeh veins.

high sulfur content, may be related to the degassing of a magmatic reservoir. This is in agreement with $\delta^{34}S$ data of a massive pyrite sample with a value close to 0‰.

Results indicate that the fluid in stage 1, with high salinity and temperature, is dominantly magmatic in origin. Boiling is a major mechanism for mineral precipitation in stage 1. During boiling, metal carrying complexes were unstable and Cu sulfide minerals were deposited. We conclude that Au was probably carried by bisulfide complexes, and because of elevated sulfur fugacity, Au remained in solution until there was a decrease in sulfur fugacity and/or an increase in oxygen fugacity during the later part of stage 1. Then the gold was deposited as inclusions in hematite. During stage 2, sulfides were deposited at approximately 245 °C under conditions of elevated sulfur fugacity (10^{-10}–$10^{-11.5}$ bars). The galena, sphalerite, chalcopyrite, and sulfosalts were deposited from a moderate salinity fluid and probably were transported in the form of chloride complexes (e.g., Henley, 1985). We assume that chlorine was magmatic in origin because of the lack of evaporites and connate brines in the region. Isothermal mixing of deep meteoric water with the magmatic hydrothermal fluid is the main mechanism for base metal deposition in stage 2 (e.g., Drummond and Ohmoto, 1985; Henley, 1985; Henley et al., 1984). Additional mixing would have occurred at shallower levels during sub-stage 2C. Mineralization in stage 3 occurred dominantly from a meteoric water. Fig. 14 shows a schematic model for mineralization in the Glojeh district.

We conclude that the heat center for mineralization is probably the Goljin intrusion located 4 km west of North Glojeh, or other intrusive bodies with ages of ~42 Ma, closer to North Glojeh. Such a heat center released magmatic fluids that traveled upwards and flowed laterally at an intermediate depth and mixed with deeply circulating meteoric water, leaching sulfur from the host rocks, and depositing the ore during three stages.

9. Conclusion

The Glojeh district is part of a silver-base metal epithermal province in Iran, and is one of the principal metal producing areas in the Tarom-Hashtjin metallogenic province. It consists of two separate mineralized vein sets, the North and the South Glojeh.

Mineral assemblages in the Glojeh veins have been grouped into three stages: An early stage (stage1) with Cu-Au-As-Sb-Fe mineralogy, a middle stage (stage 2) with Pb-Zn-Cu-Cd-Ag mineralogy, and a late stage (stage 3) with hematite-Ag-Bi-Au-Pb mineralogy. Silver-bearing minerals in the Glojeh district are native silver, tetrahedrite, Zn-tetrahedrite, Ag-tetrahedrite, greenockite, argentite, polybasite, matildite, electrum, and marrite.

The ranges of Th (150–340 °C) and salinity (0.1–11 wt.% NaCl eq.) are consistent with an epithermal environment. Fluid inclusion and stable isotope data show that Glojeh veins were deposited in a volcanic environment from a magmatic-meteoric fluid hydrothermal system. The Glojeh veins are transitional between an early high sulfidation stage (stage 1), associated with higher temperatures and salinities, and an intermediate sulfidation stage (stage 2) with slightly lower salinity and temperatures that included deposition of base metal- and silver-bearing minerals. Finally, during a late stage (stage 3), Au and Ag (Bi-Pb) were precipitated in bodies of hematite by a fluid at 160 to 200 °C and with a salinity of 0.1 to 2 wt.% NaCl eq.

The feldspar ages in two mineralized veins are concordant within error of that of the 41.87 ± 1.58 Ma Goljin intrusion that is located 4 km to the east of the North Glojeh veins. The age data provide evidence for a genetic link between the Goljin stock and the gold mineralization in the district. Results show that the North Glojeh and the South Glojeh area veins were derived from a similar fluid source, and likely resulted from multiple pulses of magmatic-hydrothermal fluid exsolving from small, shallow intrusions, which drove the hydrothermal system.

The geochemical and mineralization zoning, on local and regional scales, suggests that the heat center for the hydrothermal system is located in the north, near the North Glojeh veins. We conclude that studied veins correspond to the upper part of IS and HS epithermal systems, and there may be undiscovered resources at depth, perhaps even associated with porphyry-style mineralization.

Acknowledgments

Authors would like to thank the IMIDRO and IMPRC for technical support and Prof. Mirmohamadi Foundation (G-21390) for partial financial support. Authors also like to thank Prof. F. Pirajno and J.W. Mao for through review and constructive comments.

References

Aghazadeh, M., Castro, A., Rashidnejad Omran, N., Emami, M.H., Moinvaziri, H., Badrzadeh, Z., 2010. The gabbro (shoshonitic)–monzonite–granodiorite association of Khankandi pluton, Alborz Mountains, NW Iran. J. Asian Earth Sci. 38, 199–219.

Aghazadeh, M., Castro, A., Badrzadeh, Z., Vogt, K., 2011. Post-collisional polycyclic plutonism from the Zagros hinterland: the Shaivar Dagh plutonic complex, Alborz belt, Iran. Geol. Mag. 148, 980–1008.

Albinson, T., Norman, D.I., Cole, D., Chomiak, B.A., 2001. Controls on formation of low-sulfidation epithermal deposits in Mexico: constraints from fluid inclusion and stable isotope data. In: Albinson, T., Nelson, C.E. (Eds.), New Mines and Discoveries in Mexico and Central America. Econ Geol. Spec. Pub. Vol. 8, pp. 1–32.

Arribas, A., 1995. Characteristics of high sulfidation epithermal deposit, and their relation to magmatic fluids. In: Thompson, J.F.H. (Ed.), In Magmas, Fluids and Ore Deposits, pp. 419–456 (Chapter 19).

Arribas, A., Cunningham, C.G., Rytuba, J.J., Rye, R.O., Kelly, W.C., Podwysocki, M.H., Mckee, E.H., Tosdal, R.M., 1995. Geology, geochronology, fluid inclusion and isotope geochemistry of the Rodalquilar Au alunite deposits, Spain. Econ. Geol. 90, 795–822.

Azizi, H., Jahangiri, A., 2008. Cretaceous subduction-related volcanism in the northern Sanandaj-Sirjan Zone, Iran. J. Geodyn. 45, 178–190.

Azizi, H., Moinevaziri, H., 2009. Review of the tectonic setting of Cretaceous to Quaternary volcanism in northwestern Iran. J. Geodyn. 47, 167–179.

Bakker, R.J., 2003. Package FLUIDS 1, computer porograms for analysis of fluid inclusions data and for modeling bulk fluid properties. Chem. Geol. 194, 3–23.

Barton, P.B., Bethke, P.M., 1987. Chalcopyrite disease in sphalerite: pathology and epidemiology. Am. Mineral. 72, 451–467.

Barton, P.B., Toulmin, P., 1966. Phase relations involving sphalerite in the Fe–Zn–S system. Econ. Geol. 61, 815–849.
Beane, R.E., Titley, S.R., 1981. Porphyry copper deposits: part II. Hydrothermal alteration and mineralization. Econ. Geol. 75, 235–269.
Bente, K., Doring, T., 1993. Solid-state diffusion in sphalerites: an experimental verification of the "chalcopyrite disease". Eur. J. Mineral. 5, 465–478.
Bente, K., Doring, T., 1995. Experimental studies on the solid state diffusion of Cu and In in ZnS and on "disease", DIS (diffusion induced segregations), in sphalerite and their geological applications. Mineral. Petrol. 53, 285–305.
Bindi, L., Evain, M., Menchetti, S., 2007a. Selenopolybasite, [(Ag, Cu)6(Sb, As)2(S, Se)7][Ag9Cu(S, Se)2Se2], a new member of the pearceite-polybasite group from the De Lamar mine, Owyhee county, Idaho, USA. Can. Mineral. 45, 1525–1528.
Bindi, L., Evain, M., Spry, P.G., Menchetti, S., 2007b. The pearceite-polybasite group of minerals: crystal chemistry and new nomenclature rules. Am. Mineral. 92, 918–925.
Blourian, G.H., 1994. Petrology of Tertairy Volcanic Rocks in the North of Tehran M.Sc. thesis The university of Kharazmi, Tehran, Iran 145 p (in Persian).
Brown, P.E., 1989. FLINCOR, a microcomputer program for the reduction and investigation of fluid inclusion data. Am. Mineral. 74, 1390–1393.
Buchanan, L.J., 1981. Precious metal deposits associated with volcanic environments in the southwest. In: Dickson, W.R., Payne, W.D. (Eds.), In Relations of Tectonics to Ore Deposits in the Southern Cordillera. Ariz. Geol. Soc. Dig. Vol. 14, pp. 237–262.
Burnham, C.W., 1979. Magmas and hydrothermal fluids. In: Barnes, H.L. (Ed.), Geochemistry of Hydrothermal Ore Deposits. Wiley, New York.
Camprubí, A., Albinson, T., 2007. Epithermal deposits in Mexico: update of current knowledge, and an empirical reclassification. Geol. Soc. Spec. Pap. 422, 377–415.
Clayton, R.N., Mayeda, T.K., 1963. The use of bromine pentafluoride in the extraction of oxygen from oxides and silicates for isotopic analysis. Geochim. Cosmochim. Acta 27, 43–52.
Cooke, D.R., Simmons, S.F., 2000. Characteristics and genesis of epithermal gold deposits. Rev. Econ. Geol. 13, 221–244.
Coplen, T.B., Hopple, J.A., Böhlke, J.K., Peiser, H.S., Rieder, S.E., Krouse, H.R., Rosman, K.J.R., Ding, T., Vocke Jr., R.D., Revesz, K.M., Lamberty, A., Taylor, P., De Bièvre, P., 2002. Compilation of minimum and maximum isotope ratios of selected elements in naturally occurring terrestrial materials and reagents. U.S. Geological Survey Water-Resources Investigations Report 01-4222 (98 p).
Czamanske, G.K., 1974. The FeS content of sphalerite along the chalcopyrite-pyrite-bornite sulfur fugacity buffer. Econ. Geol. 69, 1328–1334.
Deen, J.A., Rye, R.O., Munoz, J.L., Drexler, J.W., 1994. The magmatic hydrothermal system at Julcani, Peru: evidence from fluid inclusions and hydrogen and oxygen isotopes. Econ. Geol. 89, 1924–1938.
Drummond, S.E., Ohmoto, H., 1985. Chemical evolution and mineral deposition in boiling hydrothermal systems. Econ. Geol. 80, 126–147.
Einaudi, M.T., Hedenquist, J.W., Inan, E.E., 2003. Sulfidation state of fluids in active and extinct hydrothermals systems: transitions from porphyry to epithermal environments. In: Simmons, S.F., Graham, I. (Eds.), Volcanic, Geothermal, and Ore-Forming Fluids: Rulers and Witnesses of Processes within the Earth. Econ. Geol. Spec. Pub. Vol. 10, pp. 285–313.
Gemmel, J.B., 2006. Exploration implication of hydrothermal alteration associated with epithermal Au-Ag deposits. Arc. Amirap 588, 1–5.
Gemmell, J.B., Simmons, S.F., Zantop, H., 1988. The Santo Niño Silver-Lead-Zinc vein, Fresnillo District, Zacatecas, Mexico: part I. Structure, vein stratigraphy, and mineralogy. Econ. Geol. 83, 1597–1618.
Geological Survey of Iran, 2005. Geological Map of Hashtjin: N 5664.
Ghasemi Siani, M., 2014. Timing and Origin of Epithermal Veins and Geochemical Zoning in the Glojeh District (North of Zanjan) Ph.D. thesis University of Kharazmi, Tehran, Iran (250 p. (in Persian)).
Ghasemi Siani, M., Mehrabi, B., Azizi, H., Wilkinson, C.M., Ganerod, M., 2015. Geochemistry and geochronology of the volcano-plutonic rocks associated with the Glojeh epithermal gold mineralization, NW Iran. Open Geosci. 7, 207–222.
Ghazi, A.M., Pessagno, E.A., Hassanipak, A.A., Kariminia, S.M., Duncan, R.A., Babaie, H.A., 2003. Biostratigraphic zonation and $^{40}Ar/^{39}Ar$ ages for the Neotethyan Khoy ophiolite of NW Iran. Palaeogeogr. Palaeoclimatol. Palaeoecol. 193, 311–323.
Giesemann, A., Jäger, H.J., Norman, A.L., Krouse, H.R., Brand, W.A., 1994. On-line sulfur-isotope determination using an elemental analyzer coupled to a mass spectrometer. J. Anal. Chem. 66, 2816–2819.
Haas, J.L., 1971. The effect of salinity on the maximum thermal gradient of a hydrothermal system at hydrostatic pressure. Econ. Geol. 66, 940–946.
Hedenquist, J.W., Henley, R.W., 1985. The importance of CO_2 on freezing point measurements of fluid inclusions: evidence from active geothermal systems and implications for epithermal ore deposition. Econ. Geol. 80, 1379–1406.
Hedenquist, J.W., Izawa, E., Arribas, A., White, N.C., 1996. Epithermal gold deposits: styles, characteristics and exploration. Resour. Geol. Spec. Pub. 1 (18 p.).
Hedenquist, J.W., Arribas, A.J.r., Reynolds, J.T., 1998. Evolution of an intrusion-centered hydrothermal system: far Southeast-Lepanto porphyry and epithermal Cu-Au deposits, Philippines. Econ. Geol. 93, 373–404.
Hedenquist, J.W., Arribas, A.R., Gonzalez-Urien, E., 2000. Exploration for epithermal gold deposits. Rev. Econ. Geol. 13, 245–277.
Henley, R.W., 1985. The geothermal framework for epithermal systems. Rev. Econ. Geol. 2, 1–24.
Henley, R.W., 1990. Ore Ttransport and deposition in epithermal ore environments. In: Herbert, H.K., Ho, S.E. (Eds.), Stable Isotopes and Fluid Processes in Mineralization Vol. 23. University of Western Australia, Geology Department Publication, pp. 51–69.
Henley, R.W., McNabb, A., 1978. Magmatic vapor plumes and groundwater interaction in porphyry copper emplacement. Econ. Geol. 73, 1–20.
Henley, B., Truesdell, A.H., Barton, P.B., Whitney, J.A., 1984. Fluid-mineral equilibria in hydrothermal systems. Rev. Econ. Geol. 1, 254–267.
Juteau, T., 2003. The ophiolites of Khoy (NW Iran): their significance in the Tethyan ophiolite belts of the Middle East. Compt. Rendus Geosci. 336 (2), 105–108.
khalatbari-Jafari, M., Juteau, T., Bellon, H., Whitechurch, H., Cotton, J., Emami, M.H., 2003. New geological, geochronological and geochemical investigations of the Khoy ophiolites and related formations, NW Iran. J. Asian Earth Sci. 23, 507–535.
Margolis, J., Reed, M.H., Albino, G.V., 1991. A process-oriented classification of epithermal systems: magmatic volatile-rich versus volatile poor paths [abst.]. Geol. Soc. Am. 230 (abstract 23, No 5, A).
Meheut, M., Lazzeri, M., Bala, E., Mauri, F., 2007. Equilibrium isotopic fractionation in the kaolinite, quartz, water system: Prediction from first-principles density-functional theory. Geochim. Cosmochim. Acta 71, 3170–3181.
Mehrabi, B., Ghasemi Siani, M., Azizi, H., 2014. The genesis of the epithermal gold mineralization at North Glojeh veins, NW Iran. IJSAR 15 (1), 479–497.
Mirnejad, H., Hassanzadeh, J., Cousens, B.L., Taylor, B.E., 2010. Geochemical evidence for deep mantle melting and lithospheric delamination as the origin of the inland Damavand volcanic rocks of Northern Iran. J. Volcanol. Geotherm. Res. 198, 288–296.
Moayyed, M., 2001. Investigation of Tertiary Volcano-Plutonic Bodies in West Alborz-Azarbayejan (Hashtjin Area) Ph.D. thesis University of Shahid Beheshti, Tehran, Iran (296 p. (in Persian)).
Nabatian, G., Ghaderi, M., 2013. Oxygen isotope and fluid inclusion study of the Sorkhe-Dizaj iron oxide-apatite deposit, NW Iran. Int. Geol. Rev. 55, 397–410.
Nabatian, G., Ghaderi, M., Neubauer, F., Honarmand, M., Liu, X., Dong, Y., Jiang, S., Quadet, A., Bernroider, M., 2014. Petrogenesis of Tarom high-potassic granitoids in the Alborz–Azarbaijan belt, Iran: geochemical, U–Pb zircon and Sr–Nd–Pb isotopic constraints. Lithos 184-187, 324–345.
Norman, D.I., Chomiak, B., Albinson, T., Moore, J.N., 1997b. Volatiles in epithermal systems: the big picture. GSA 1997 Annual Meeting, Abstracts with Programs, A-206.
Pudack, C., Halter, W.E., Heinrich, C.A., Pettke, T., 2009. Evolution of magmatic vapor to gold-rich epithermal liquid: the porphyry to epithermal transition at Nevados de Famatina, Northwest Argentina. Econ. Geol. 104, 449–477.
Roedder, E., Bodnar, R.J., 1980. Geologic pressure determinations from fluid inclusions studies. Annu. Rev. Earth Planet. Sci. 8, 263–301.
Rye, R.O., Bethke, P.M., Wasserman, M.D., l992. The stable isotope geochemistry of acid-sulfate alteration. Econ. Geol. 87, 225–267 1992.
Scott, S.D., Barnes, H.L., 1971. Sphalerite geothermometry and geobarometry. Econ. Geol. 66, 653–669.
Scott, S.D., Kissin, S.A., 1973. Sphalerite composition in the Zn–Fe–S system below 300 °C. Econ. Geol. 68, 475–478.
Sillitoe, R.H., 1999a. Styles of high-sulfidation gold, silver and copper mineralization in the porphyry and epithermal environments. In: Weber, G. (Ed.), Pacrim '99 Congress, Bali, Indonesia, 1999, Proceedings: Parkville. AIMM, pp. 29–44.
Sillitoe, R.H., Hedenquist, J.W., 2003. Linkages between volcanotectonic settings, ore fluid compositions, and epithermal precious-metal deposits. Econ. Geol. Spec. Pub. 10, 315–343.
Sillitoe, R.H., Steele, G.B., Thompson, J.F.H., Lang, J.R., 1998. Advanced argillic lithocaps in the Bolivian tin-silver belt. Mineral. Deposita 33, 539–546.
Simon, G., Kesler, S.E., Essene, E.J., 1997. Phase relations among selenides, sulfides, tellurides, and oxides: II. Applications toselenide-bearing ore deposits. Econ. Geol. 92, 468–484.
Steele, G.B., 1996. Metallogenesis and Hydrothermal Alteration at Cerro Rico, Bolivia Ph.D. thesis University of Aberdeen, Aberdeen (435 p.).
Stoffregen, R.E., 1987. Genesis of acid-sulfate alteration and Au-Cu-Ag mineralization at Summitville, Colorado. Econ. Geol. 82, 1575–1591.
Vallance, J., Cathelineau, M., Boiron, M.C., Fourcade, S., Shepherd, T.J., Naden, J., 2003. Fluid–rock interactions and the role of late Hercynian aplite intrusion in the genesis of the Castromil gold deposit, Northern Portugal. Chem. Geol. 194, 201–224.
Vallance, J., Boiron, M., Cathelineau, M., Fourcade, S., Varlet, M., Marignac, C., 2004. The granite hosted gold deposit of Moulin de Cheni (Saint-Yrieix district, Massif central, France): petrographic, structural, fluid inclusion and oxygen isotope constraints. Mineral. Deposita 39, 265–281.
Velador, J.M., 2010. Timing and Origin of Intermediate Sulfidation Epithermal Veins and Geochemical Zoning in the Fresnillo District, Mexico: Constrained by $^{40}Ar/^{39}Ar$ Geochronology, Fluid Inclusions, Gas Analysis, Stable Isotopes, and Metal Ratios Ph.D thesis New Mexico Institute of Mining and Technology, Department of Earth and Environmental Sciences (185p.).
Wallace, A.B., 1980. Geochemistry of polymetallic veins and associated wall rock alteration, Pyramid district, Washoe County, Nevada. Mine. Eng. 32, 314–320.
White, N.C., Hedenquist, J.W., 1990. Epithermal environments and styles of mineralization: variations and their causes, and guidelines for exploration. J. Geochem. Explor. 36, 445–474.
Wilkinson, J.J., 2001. Fluid inclusion in hydrothermal ore deposit. Lithos 55, 229–272.
Williams-Jones, A.E., Heinrich, C.A., 2005. Vapor transport of metals and the formation of magmatic-hydrothermal ore deposits: 100th anniversary spec. Pap. Econ. Geol. 100, 1287–1312.